Geological Society of America Bulletin

Impacts of Cenozoic global cooling, surface uplift, and an inland seaway on South American paleoclimate and precipitation $\delta^{18}O$

M. Louise Jeffery, Christopher J. Poulsen and Todd A. Ehlers

Geological Society of America Bulletin 2012;124, no. 3-4;335-351
doi: 10.1130/B30480.1

Notes

Impacts of Cenozoic global cooling, surface uplift, and an inland seaway on South American paleoclimate and precipitation $\delta^{18}O$

M. Louise Jeffery[1,†], Christopher J. Poulsen[1], and Todd A. Ehlers[2,1]
[1]*Department of Earth and Environmental Sciences, University of Michigan, Ann Arbor, Michigan 48109, USA*
[2]*Department of Geosciences, Universität Tübingen, 72074 Tübingen, Germany*

ABSTRACT

Stable isotope records of precipitation $\delta^{18}O$ ($\delta^{18}O_{prec}$) have been used as paleoclimate and paleoelevation archives of orogens. However, interpretation of these records is limited by knowledge of how $\delta^{18}O_{prec}$ responds to changes in global and regional climate during mountain-building events. In this study the influence of atmospheric CO_2 levels, the extent of the Antarctic ice sheet, changes in Andean surface elevation, and the presence of the South American inland seaway on climate and $\delta^{18}O_{prec}$ in South America are quantified using the GENESIS v3 atmospheric general circulation model with isotope-tracking capabilities. Results are presented in the context of Cenozoic South American climate and $\delta^{18}O_{prec}$ changes. More specifically, we find: (1) Precipitation rates in the Andes are sensitive to Andean surface elevation, the seaway and, to a lesser extent, CO_2 levels. Increasing Andean elevations and the presence of a seaway both cause large increases in precipitation, but in different parts of the Andes. The growth of the Antarctic ice sheet is found to have a small influence on South American precipitation. (2) The stable isotopic composition of precipitation is sensitive to all of the parameters investigated. An increase in $\delta^{18}O_{prec}$ of up to 8‰ is found in simulations with higher atmospheric CO_2. In agreement with previous studies, $\delta^{18}O_{prec}$ decreases with increasing Andean elevation by an amount greater than that predicted by the modern adiabatic lapse rate. Furthermore, the presence of an inland seaway causes a decrease in $\delta^{18}O_{prec}$ of 1–8‰ in the northern and central Andes. The amount of depletion is dependent on the isotopic composition of the seaway. Simulations without the Antarctic ice sheet result in $\delta^{18}O_{prec}$ that is 0–3‰ lower than the modern. Finally, time-specific simulations for the Miocene and Eocene show that $\delta^{18}O_{prec}$ has decreased during the Cenozoic and that local geographical gradients of $\delta^{18}O_{prec}$ have increased, particularly in regions of high modern elevation. We demonstrate that in addition to Andean uplift and associated climate change, CO_2 levels and an inland seaway are likely to have influenced $\delta^{18}O_{carb}$ records from South America. Consideration of these global and paleogeographic changes is necessary when interpreting paleoclimate or paleoelevation from stable isotope records of $\delta^{18}O_{prec}$.

INTRODUCTION

The Cenozoic was a time of major mountain building events and global cooling of ~10 °C (Lear et al., 2000). These events altered global atmospheric circulation patterns and led to polar glaciation (Ehrmann and Mackensen, 1992; Zachos et al., 1992). These large-scale changes should be recorded in stable isotope records from orogenic regions. However, unraveling these signals is difficult, partly because the isotopic responses to changing geologic boundary conditions are not well constrained. Isotope-tracking climate models can be used to determine the response of the stable isotopic composition of precipitation ($\delta^{18}O_{prec}$) to changes in boundary conditions. The advantage to such an approach is that the spatial response to individual factors (e.g., surface uplift, global cooling, or Antarctic glaciation) can be quantified.

Recent studies of the Andean Plateau have highlighted that terrestrial paleosol and lacustrine carbonate stable isotope ($\delta^{18}O_{carb}$) records from South America are sensitive to both the paleoelevation and paleoclimate history of the orogen (Ehlers and Poulsen, 2009; Poulsen et al., 2010). These studies demonstrated how increasing Andean Plateau elevations and consequent climate change alter $\delta^{18}O_{prec}$. However, global or regional climate and environmental changes that occurred during the evolution of the Andes were not taken into account. Furthermore, episodic occurrences of a marine seaway or freshwater lake in the Andean foreland have modified the regional paleogeography during the Cenozoic (Frailey et al., 1988; Rasanen et al., 1995). A better understanding of the impacts of these global and regional changes, as well as the impacts of changing Andean Plateau elevations, on $\delta^{18}O_{prec}$ in South America is needed in order to accurately interpret $\delta^{18}O_{carb}$ records from this region.

In this study, we complement previous work by using a global climate model with isotopic tracking capabilities to quantify the impacts of global climate and paleogeographic change on the isotopic composition of meteoric waters. We establish the relative importance of (1) atmospheric greenhouse gas (CO_2) composition, (2) the Antarctic ice sheet, (3) Andean elevation, and (4) the presence of a South American inland seaway on the climate and $\delta^{18}O_{prec}$ in South America. We use these results to show the paleoclimate and paleoelevation signals that may be observed in $\delta^{18}O_{carb}$ records of South America.

BACKGROUND

South American Paleogeography and Paleoclimate

The ~7000-km-long Andean mountains (Fig. 1) formed primarily as a result of the subduction of the Nazca plate beneath the South American plate. The morphology of the Andes varies considerably along strike with narrow ranges to the north and south separated by the wide Altiplano plateau of the central Andes (15–27 °S, Fig. 1; Isacks, 1988). South America has been located in the lower latitudes for the past 40 Ma and has drifted northwards by ~2° since 10 Ma (Smith et al., 1981).

In the following we briefly summarize the evolution of this orogen from south to north. In the southern Patagonian Andes, accelerated

†E-mail: louisej@umich.edu

GSA Bulletin; March/April 2012; v. 124; no. 3/4; p. 335–351; doi:10.1130/B30480.1; 8 figures; 1 table; Data Repository item 2011326.

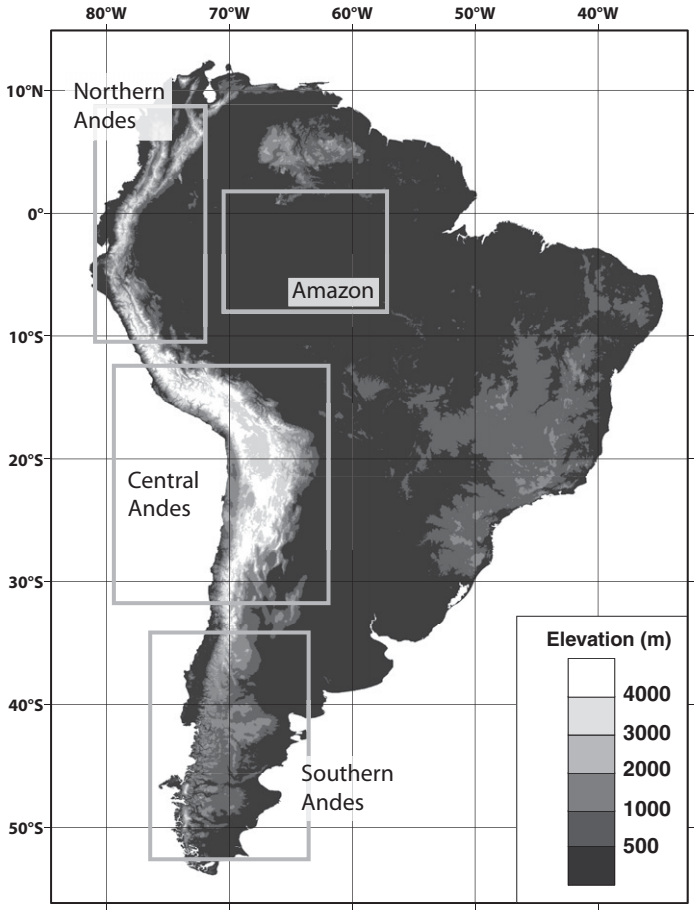

Figure 1. Modern South American topography. Boxes delineate the regions discussed in the text.

cooling and denudation began ca. 30 Ma (Thomson et al., 2001) and indicates the onset of significant deformation in this region. Deformation propagated eastward before slowing at 14–10 Ma following the subduction of the Chilean spreading ridge (Blisniuk et al., 2006). The Pampean segment of the Andes (27–33 °S) is distinguished by a gap in modern volcanism over a region of flat-slab subduction. Here, the main deformation phase in the principal Cordillera occurred between 20 and 8.6 Ma (Ramos et al., 2002). Again, deformation propagated eastward from the main Cordillera into the Sierra Pampeanas fold-and-thrust belt. In the central Andes, deformation began in the early Cenozoic (60–40 Ma, DeCelles and Horton, 2003; McQuarrie et al., 2005) and accelerated ca. 25 Ma coincident with a change in the subduction geometry. The plateau formed mainly through crustal thickening and deformation that migrated eastward from the Altiplano-Puna Plateau into the foreland fold-and-thrust belt (Barnes et al., 2008; McQuarrie, 2002). Deformation in the Altiplano began 5–10 m.y. before the Puna region (Allmendinger et al., 1997). North of the Altiplano, the Andean range narrows and splits into three separate Cordilleras (north of 2° N, Fig. 1). The northern Andes have a long history of deformation that is complicated by the subduction of the proto–Caribbean plate in addition to the Nazca plate (Gómez et al., 2005; Taboada et al., 2000). Earliest contractional deformation began in the Late Cretaceous when accretion of an oceanic plateau initiated formation of the Western Cordillera and contemporaneous arc volcanism and crustal thickening began in the Central Cordillera. After plate reorganization at ca. 28–26 Ma, basin inversion in the foreland led to the uplift of the Eastern Cordillera in the late Oligocene and early Miocene (Cooper et al., 1995; Parra et al., 2010).

Central South America was episodically submerged under fresh or marine waters during the Neogene. Sedimentary evidence from the Andean foreland indicates the presence of a large lake (Frailey et al., 1988) or an inland seaway during the Miocene (Rasanen et al., 1995). Miocene sedimentary deposits from Peruvian Amazonia are interpreted to have formed in a range of environments from fluvial (Latrubesse et al., 2010) to marginal marine (Gingras et al., 2002; Rasanen et al., 1995). Evidence for a marine influence includes diurnal cycles in rhythmic bedding (Hovikoski et al., 2007; Hovikoski et al., 2005), mangrove pollen (Hoorn, 2006), marine palynmorphs (Hoorn, 2006), marine ichnofossils (Gingras et al., 2002; Wesselingh et al., 2002), and a high diversity of modern marine-derived fauna (Lovejoy et al., 2006). Others have interpreted the sedimentary structures as a fluvial system with avulsive rivers, megafans, swamps, and lakes (Latrubesse et al., 2010). The conflicting evidence for continental and marine influences in the same formation can be reconciled by a scenario in which multiple incursions of brackish water occurred into an otherwise continental environment (Hovikoski et al., 2007; Hovikoski et al., 2010; Wesselingh et al., 2006). In a recent review, Hoorn et al. (2010) describe the following three phases of seaway incursions in Amazonia; (1) ca. 24–16 Ma: lacustrine conditions alternating with episodes of fluvial drainage and marginal marine influence; (2) ca. 16–11.3 Ma: maximum extent of lacustrine conditions with a marginal marine influence; and (3) 11.3–ca. 7 Ma: complex environment of deltaic, estuarine, and fluvial environments. Probable causes of the incursions include tectonic loading of the foreland basin by the rising Andes and/or changes in eustatic sea level (Hernandez et al., 2005).

These paleogeographic changes all occurred in the context of Cenozoic global climate change. Carbon dioxide levels and global temperatures have decreased throughout the Cenozoic. Carbon dioxide concentrations were ~900–1500 ppm in the middle to late Eocene (Pagani et al., 2005; Pearson et al., 2009) but have been relatively stable below ~500 ppm since the late Oligocene, ca. 25 Ma (Demicco et al., 2003; Royer, 2006). The Antarctic ice sheet initially developed ca. 34 Ma (Matthews and Poore, 1980; Miller et al., 1987; Zachos et al., 1992) and fluctuated in size through the Oligocene and Miocene. The Eastern Antarctic ice sheet stabilized ca. 14 Ma, and the modern ice sheet was established in the Plio-Pleistocene (Siegert et al., 2008).

The Isotopic Composition of South American Precipitation

The isotopic composition of meteoric water is primarily controlled by equilibrium isotopic fractionation during evaporation and precipitation (Gat, 1996). It is energetically more favorable for molecules containing the lighter isotope (^{16}O) to be in the gaseous phase. Therefore,

precipitation is more enriched in ^{18}O than the vapor from which it formed, and the remaining vapor becomes isotopically depleted. This fractionation is temperature dependent, with greater fractionation occurring at lower temperatures (Dansgaard, 1964).

In South America, $\delta^{18}O_{prec}$ decreases generally from north to south, particularly south of 45 °S, due to decreasing temperature with increasing latitude (Rozanski et al., 1993). The $\delta^{18}O_{prec}$ is also more negative inland than at the coasts as a result of Rayleigh distillation, the progressive rainout of the heavier isotope. These continental effects are weaker in the Amazon region due to recycling through evapotranspiration of moisture with relatively high $\delta^{18}O_{prec}$ (Salati et al., 1979). A minimum in the $\delta^{18}O_{prec}$ pattern occurs in eastern Brazil (40–50 °W, 20 °S) due to high precipitation rates and long vapor transport distances over which Rayleigh distillation occurs.

Further modifications to the general latitudinal and continental pattern are caused by the presence of the Andean topography (Aravena et al., 1999; Gonfiantini et al., 2001; Stern and Blisniuk, 2002). The lifting of air masses over high topography induces adiabatic cooling and condensation on the windward side resulting in more isotopically depleted precipitation at high elevation and on the leeward side of the mountain range (Dansgaard, 1964). Elevation effects are particularly strong in the central Andes, where the South American low-level jet stream brings moisture southwards, and convective precipitation is induced on the eastern Andean flanks (Insel et al., 2009).

METHODS

Modeling Approach

A suite of climate-model simulations (Table 1) is used to explore the response of South American climate and $\delta^{18}O_{prec}$ to a range of climate controls that have changed during the mid-late Cenozoic. The simulations were run using the global climate model GENESIS (Thompson and Pollard, 1995, 1997). GENESIS is a multicomponent Earth systems model with an atmospheric model derived from the National Center for Atmospheric Research's CCM1 coupled to land-surface, soil, snow, sea-ice, and ocean components. In our version of GENESIS, water isotopic transport and fractionation processes have been added to the atmospheric physics (Mathieu et al., 2002). The $^{18}O/^{16}O$ and D/H ratios are predicted in atmospheric vapor, liquid, and ice, and also in soil-water reservoirs. Fractionation is modeled as a result of condensation and evaporation in the free atmosphere and from surface waters. Atmospheric isotopic ratios are transported using the same Lagrangian transport as for bulk vapor and clouds. We use a spectral resolution of T63 (~1.9° or ~210 km) for both the atmosphere and surface models. The atmospheric model has 18 vertical levels. Vegetation cover is prescribed based on Dorman and Sellers (1989) and is identical in each simulation. The ocean is represented by a mixed-layer slab model of 50-m depth. Oceanic heat transport is diffusive and zonally uniform. Atmospheric trace-gas compositions are specified at preindustrial levels, except for carbon dioxide as described below. The isotopic composition of the oceans and other large water bodies is prescribed from modern observational data sets (Craig and Gordon, 1965; Epstein and Mayeda, 1953; Ferronsky and Brezgunov, 1989; GEOSECS, 1987). Orbital parameters are modern and constant in all experiments.

Each simulation was run for 55 years with isotope tracking enabled for the last 25 years. The results presented here were averaged over the final 20 years of each simulation. Twenty years is sufficient time to establish the mean climatic state because the use of a slab ocean does not enable the simulation of the ocean-atmosphere interactions that drive variability on annual and longer time scales in the modern climate. While this is a limitation of this study, the slab-ocean model was chosen in order to maintain surface-temperature equilibrium under increasing CO_2 levels. Furthermore, interannual variability is unlikely to be recorded in carbonate records of $\delta^{18}O_{prec}$ that form over comparatively long time periods of hundreds to thousands of years. Additionally, the changes in boundary conditions that we explore occur on time scales greater than that of carbonate formation.

TABLE 1. MODEL EXPERIMENTS AND BOUNDARY CONDITIONS

	Full Andes	Half Andes	No Andes
1× CO_2	Modern SW_{marine} $SW_{freshwater}$ NoIce NoIce_modOcean (GSA DR)	Half Andes (GSA DR) Half Andes, SW_{marine} (GSA DR)	No Andes
2× CO_2	2× CO_2 (GSA DR)	Middle Miocene 2× CO_2, Half Andes (GSA DR)	
4× CO_2	4× CO_2		Eocene (NoIce, Ocean)

SW—Seaway; marine—marine isotopic composition (~1‰); freshwater—freshwater isotopic composition (–6‰); NoIce—topography and surface properties of the Antarctic ice sheet changed and ocean isotopic composition modified for an ice-free world; NoIce_modOcean—Antarctic topography and surface properties changed, but oceanic isotopic composition is modern; $N \times CO_2$—CO_2 levels at N times preindustrial level (280 ppm); GSA DR—GSA Data Repository (see footnote 1). Experiment results are shown in the Data Repository (see footnote 1) available online.

Cenozoic Boundary Conditions

A series of simulations were completed that investigate the impact of (1) atmospheric CO_2 levels, (2) Andean elevation, (3) the South American Inland Seaway, and (4) the Antarctic ice sheet on $\delta^{18}O_{prec}$ in South America. Boundary conditions were specified to capture the range of conditions during the Cenozoic. The set of simulations (Table 1) consists of a base level, or control run, representing preindustrial conditions and further simulations in which only one parameter is varied from the base-level conditions. The exceptions to this are two time-specific simulations discussed at the end. The CO_2 levels in the base-level simulation are 1× that of preindustrial levels (PIL) (280 ppm). Additional simulations are run at 2× (560 ppmv) and 4× (1120 ppmv) PIL (Pagani et al., 2005; Pearson et al., 2009). The influence of Andean surface uplift is examined with simulations at varying Andean elevations. Figure 2A shows the modern Andean topography represented in the "Full Andes" simulations. Two additional experiments were completed with modern Andean elevations reduced by 50% ("Half Andes") and set to 250 m ("No Andes").

We have adapted a seaway reconstruction (Fig. 2A) modified from Hernandez et al. (2005) and Rasanen et al. (1995). The reconstruction represents the maximum likely extent of the seaway. The isotopic composition of the seaway is not known, in part because it is not clear whether the seaway had a marine connection. To address this uncertainty, two experiments were conducted with distinct isotopic compositions assigned to the seaway ($\delta^{18}O_{seaway}$). The first experiment representing a marine seaway has isotopic compositions similar to the modern Atlantic with zonal values ranging from 1‰ near the equator to 0‰ at 50 °S. The second experiment represents a freshwater seaway with an isotopic composition of –6‰, the value of the modern Amazon River. The "marine" scenario could also represent a freshwater seaway that has undergone high rates of evaporation. These two simulations (SW_{marine} and $SW_{freshwater}$) encompass the range of potential influences a seaway could have on the $\delta^{18}O_{prec}$ in South America.

Changes in Antarctic ice volume influence $\delta^{18}O_{prec}$ by modifying the climate and by changing

oceanic isotopic composition ($\delta^{18}O_{ocean}$). Our NoIce experiment simulates this using an ice-free isostatically rebounded Antarctic paleogeography. The $\delta^{18}O_{ocean}$ is prescribed by subtracting 1.2‰ from modern $\delta^{18}O_{ocean}$ values. The NoIce experiment tests the maximum impact of the Antarctic ice sheet on $\delta^{18}O_{prec}$ for the Cenozoic because the Antarctic ice sheet is completely removed. An additional experiment (NoIce_modOcean, Table 1) explores the relative importance of climate and $\delta^{18}O_{ocean}$ changes to differences in $\delta^{18}O_{prec}$ in the absence of the Antarctic ice sheet. In this experiment the Antarctic ice sheet is removed, but $\delta^{18}O_{ocean}$ is set to modern values. The Greenland ice sheet was not modified in our experiments. Due to its distant location from South America, the topography and surface type of the Greenland ice sheet would have a very small effect on $\delta^{18}O_{prec}$ in South America compared to the other boundary conditions explored here.

In addition to sensitivity tests of the boundary conditions described above, two time-specific simulations were designed to represent the (1) late Eocene (ca. 40 Ma) and (2) middle Miocene (ca. 15 Ma). The Eocene scenario has no Antarctic ice sheet, an ice-free world $\delta^{18}O_{ocean}$, 4× CO_2 (1120 ppm), and No Andes elevation. The Miocene scenario has a modern Antarctic ice sheet, modern $\delta^{18}O_{ocean}$, 2× CO_2 (560 ppm), and Half Andes elevation. All simulations and their boundary conditions are summarized in Table 1.

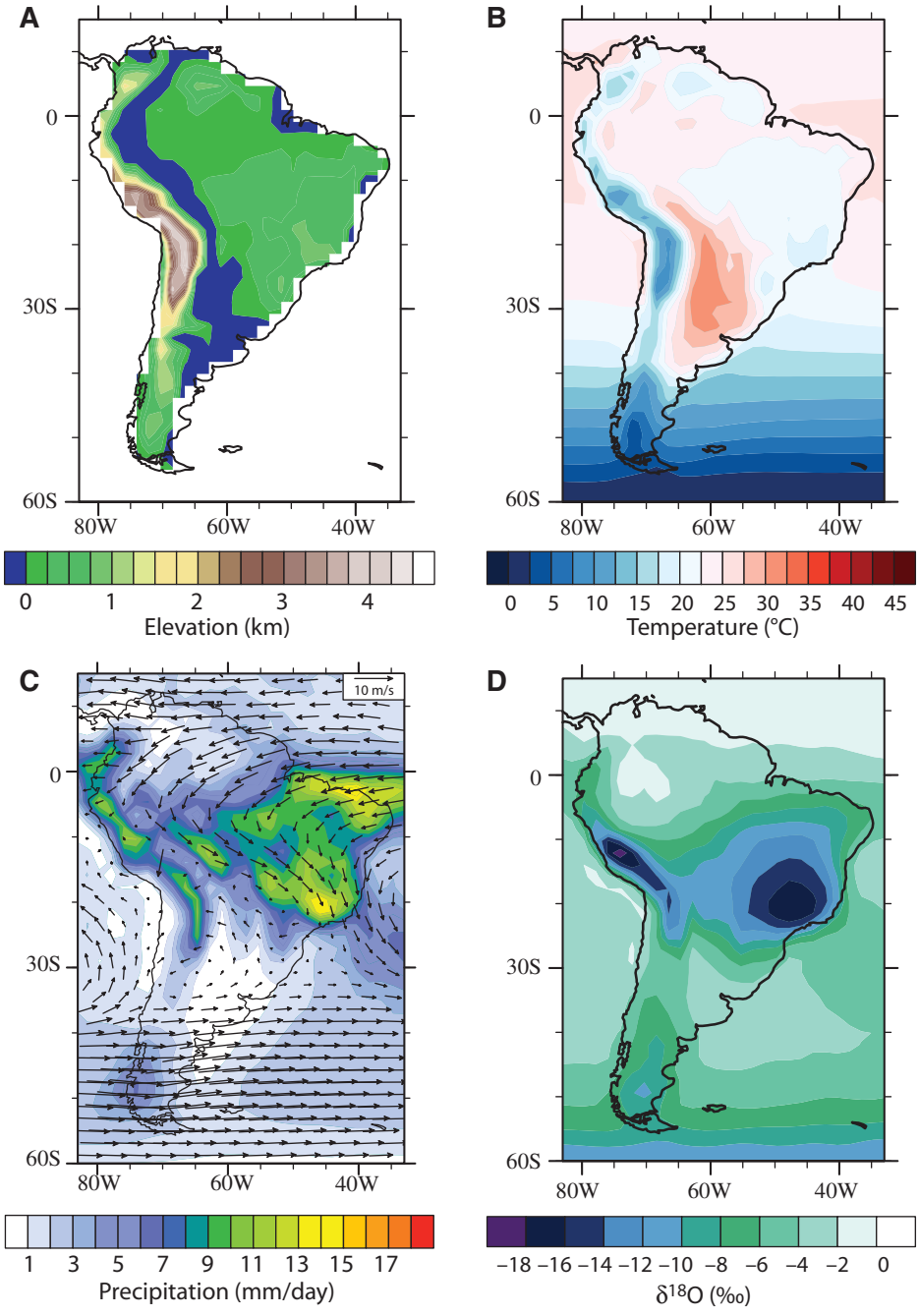

Figure 2. Model topography and austral summer climatologies for the modern simulation. (A) GENESIS modern South America topography. The location of the South American interior seaway is indicated by blue shading. The seaway is incorporated only in the $SW_{freshwater}$ and SW_{marine} simulations (see Table 1). (B) Summer (December-January-February [DJF]) average surface temperatures (°C). (C) Summer (DJF) average precipitation (mm/day) and 800 mb winds (m/s). Winds are not shown where surface elevation exceeds 2000 m. (D) Simulated amount-weighted summer $\delta^{18}O_{prec}$ (‰).

RESULTS

Modern (Control) Simulation

GENESIS has been used to realistically simulate both modern and past climates (e.g., Sloan et al., 1996; Thompson and Pollard, 1995; Zhou et al., 2008). South American climate simulated in the control run compares well with modern data (Fig. 3, CMAP, CRU TS 2.0, NCEP 1, Kalnay et al., 1996; Pearson and Palmer, 2000; Xie and Arkin, 1997). For example, temperatures of ~25 °C in the Amazon and cooler temperatures (<10 °C) at high elevation and high latitudes (south of 40 °S) compare well with observational data (Figs. 3A–3C). Predicted and observed precipitation patterns agree well, with high-precipitation rates in the Amazon (3–6 mm/day) and northern and central Andes (up to 12 mm/day). GENESIS also captures low-precipitation rates (<3 mm/day) at 30–40 °S (Figs. 3D–3F). Discrepancies between the model and observations occur in eastern Brazil, where the model overestimates precipitation rates by up to 4 mm/day. This is likely due to local sea-surface temperatures being too high as a result of using the slab-ocean model. Precipitation rates are also slightly too high on the eastern flanks of the Andes.

Modern $\delta^{18}O_{prec}$ patterns are well represented in the control simulation (Fig. DR4A[1]) when compared with currently available, and

[1]GSA Data Repository item 2011326, DR1: Results of additional experiments and DR2–5: Mean annual and seasonal results, is available at http://www.geosociety.org/pubs/ft2011.htm or by request to editing@geosociety.org.

sparse, observational data sets (International Atomic Energy Agency and World Meteorological Organization, 1998–2010); Mathieu et al., 2002; Poulsen et al., 2010). The $\delta^{18}O_{prec}$ is high (>–6‰) over much of the Amazon basin and is low (<–10‰) in the central Andes, southeastern Brazil (40–50 °W, 20 °S), and in the southern Andes. Both the patterns and magnitude of $\delta^{18}O_{prec}$ are similar to those simulated in other climate models of a similar resolution (Vuille et al., 2003) and higher resolution (Sturm et al., 2007; Vuille et al., 2003). Any errors in climate simulation propagate into errors in $\delta^{18}O_{prec}$ simulation. As a result, GENESIS may under- or over-estimate the magnitude of $\delta^{18}O_{prec}$ where

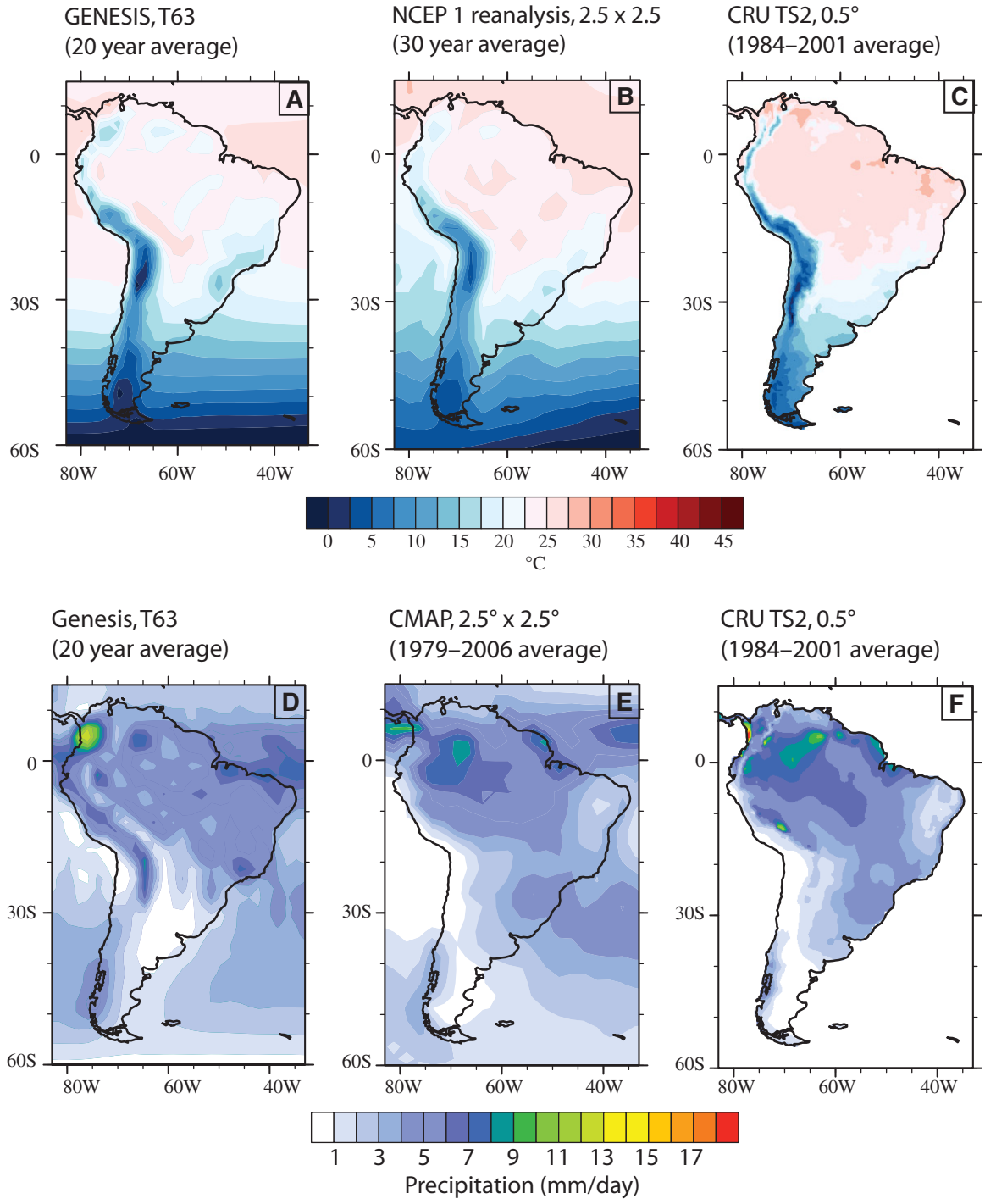

Figure 3. Model performance. Simulated and observed mean annual temperature (°C) (A–C) and precipitation (mm/day) (D–F). (A and D) GENESIS (this paper); (B) National Centers for Environmental Prediction (NCEP) 1 reanalysis product at 2.5° resolution; (C and F) Climate Research Unit (CRU) TS2.0 at 0.5° resolution; and (E) Climate Prediction Center (CPC) Merged Analysis of Precipitation (CMAP) at 2.5° resolution.

precipitation rates or temperatures are not well simulated. In eastern Brazil for example, simulated precipitation rates are too high, which results in an underestimate of $\delta^{18}O_{prec}$. However, much of this paper focuses on the Andes, where the model successfully simulates a decrease in $\delta^{18}O_{prec}$ from ~–6‰ at low elevations to as low as <–16‰ on the eastern central Andean flanks (Fig. DR4A [see footnote 1]), comparable to modern meteoric waters. Observed stream water and precipitation $\delta^{18}O$ decreases from ~–2 to –8‰ at low elevations to ~–11 to –18‰ at ~5 km elevation (Bershaw et al., 2010; Gonfiantini et al., 2001). At 33 °S, river waters thought to reflect winter $\delta^{18}O_{prec}$ have values of –3‰ to –5‰ at low elevations, decreasing to ~–18‰ at 4-km elevation (Hoke et al., 2009). In GENESIS austral winter $\delta^{18}O_{prec}$ ranges from –6‰ to –14‰ at the same latitude (Fig. DR4 [see footnote 1]). Simulated $\delta^{18}O_{prec}$ is also comparable to observations from the Patagonian Andes (47–48 °S, Stern and Blisniuk, 2002). At these two southerly locations, the most depleted values may not be well simulated because the model is too coarse to represent the full elevation where the range is narrow. We consider the model acceptable for the following experiments because it captures the important large-scale features of climate and $\delta^{18}O_{prec}$ in South America. We show our results in comparison to the control run in order to highlight the impact of particular changes in boundary conditions and to minimize the error in the results.

Sensitivity Experiments

For each change in model parameters, we present the changes in South American regional climate (Fig. 4) and $\delta^{18}O_{prec}$ (Fig. 5). The main results discussed here are 20-yr austral summer (December-January-February [DJF]) averages. Because austral summer is the wet season in the central Andes, it dominates the weighted-mean annual average $\delta^{18}O_{prec}$ signal. The central Andes is also where many $\delta^{18}O_{prec}$ records and paleoaltimetry studies are focused. Because DJF is not the dominant rainfall season in other parts of South America, we also show mean annual (Fig. 6) and austral winter (Figs. DR2–DR5 [see footnote 1]) results.

CO_2 Effects on $\delta^{18}O_{prec}$

The global mean annual temperatures (MATs) are 12.6 °C, 15.4 °C, and 19.1 °C in the control (1× CO_2), 2× CO_2, and 4× CO_2 simulations, respectively. The temperature increase of ~2.8 °C between 1× and 2× CO_2 is consistent with other models and observational data sets (Knutti et al., 2006; Murphy et al., 2004). Temperature increases are not spatially uniform (Fig. 4E), with temperatures increasing more over land than over the oceans. At 4× CO_2, warming of 4–6 °C in the low-latitude ocean is accompanied by an increase of 8–10 °C in the center of the continent and an increase of 6–8 °C on the central Andean plateau. At 4× CO_2, precipitation decreases by up to 3–4 mm/day in the central Andean foreland and increases by up to 6–8 mm/day on the northeast coast (Fig. 4A).

At higher CO_2 levels, $\delta^{18}O_{prec}$ increases across South America with the exception of the Amazon basin (Fig. 5A). The maximum change occurs in the central Andes, where $\delta^{18}O_{prec}$ is –8‰ (Fig. 5A) at 4× CO_2, 6–8‰ (Fig. 5F) less negative than the modern. In the southern Andes, $\delta^{18}O_{prec}$ is between –6‰ and –8‰ in the 4× CO_2 simulation, 2–3‰ less negative than in the control simulation. Increases in $\delta^{18}O_{prec}$ can be attributed primarily to temperature controls (Fig. 4E) on the amount of kinetic fractionation and to a lesser degree to changes in precipitation (Fig. 4A), which alter the amount of rainout. At higher temperatures, isotopic fractionation during surface evaporation and cloud condensation is reduced. The specific humidity is also higher, which, according to distillation principles, leads to less negative $\delta^{18}O_{vapor}$. For the same precipitation pattern, the $\delta^{18}O$ of water vapor is therefore less negative than the control simulation throughout the vapor transport path. In the Amazon region, $\delta^{18}O_{prec}$ is –2‰ to –6‰, 1‰–3‰ more negative than in the control simulation. This decrease can be attributed to an increase in precipitation that enhances Rayleigh distillation. These effects of increased precipitation rates on $\delta^{18}O_{prec}$ are geographically restricted. As the prevailing winds (Fig. 2C) transport depleted moisture from the northeast coast of Brazil westwards across the Amazon basin and toward the central Andes, high temperatures and mixing with less depleted air masses counteract the depletion caused by high rainout rates over the Atlantic (Fig. 4A). At 2× CO_2, the changes in precipitation, temperature, and $\delta^{18}O_{prec}$ (Figs. DR1A and DR1F [see footnote 1]) relative to the control simulation are smaller in magnitude than at 4× CO_2 but follow a similar pattern.

Andean Elevation Effects on $\delta^{18}O_{prec}$

In agreement with other studies (Campetella and Vera, 2002; Ehlers and Poulsen, 2009; Insel et al., 2009; Lenters and Cook, 1995), the elevation of the Andes is shown to exert a strong control on the regional climate. In the No Andes simulation, precipitation (Fig. 4B) decreases by 8 mm/day on the eastern flanks of the central Andes and increases in the western Amazon basin by 3–5 mm/day compared to the control simulation. Temperatures increase by 20–25 °C in the central Andes when the Andes are lowered but remain constant in regions where elevation is identical in both simulations (Fig. 4F).

The $\delta^{18}O_{prec}$ in the northern, central, and southern Andes is 2–3‰, 4–8‰, and 2–3‰, respectively, less negative in the No Andes experiment than in the control simulation (Fig. 5G). The opposite signal is observed in the Amazon basin; $\delta^{18}O_{prec}$ is more negative by as much as 4–6‰ in the No Andes simulation (Fig. 5G). The Half Andes simulation shows a similar pattern of change as a result of elevation decrease but of a smaller magnitude (Figs. DR1B and DR1G [see footnote 1]).

In the Amazon basin the higher precipitation rates at lower Andean elevation result in more negative $\delta^{18}O_{prec}$. In the northern and central Andes, changes in adiabatic cooling, amount effects, and moisture source all play a role in determining $\delta^{18}O_{prec}$. In the central Andes and north of the equator, an increase in precipitation (Fig. 4B) with increasing elevation enhances the decrease in $\delta^{18}O_{prec}$ expected from adiabatic cooling alone. In addition, as elevations increase, the Andes act as a barrier to zonal circulation and prevent moisture derived from the Pacific from penetrating inland resulting in greater influence from Atlantic-sourced moisture (Insel et al., 2009). In western South America, Pacific-sourced water has a shorter travel distance and undergoes less Rayleigh distillation than Atlantic-sourced water vapor, causing it to be less depleted. Switching from a Pacific to Atlantic moisture source therefore results in more negative $\delta^{18}O_{prec}$. In the southern Andes, where a slight increase in precipitation (1–2 mm/day at 50 °S, Fig. 4B) accompanies uplift and there is no change in moisture source (GEOSECS, 1987), the increase in $\delta^{18}O_{prec}$ with increasing elevation is weaker than in the central Andes and dominated by adiabatic cooling effects.

Seaway Effects on $\delta^{18}O_{prec}$

The seaway exerts a strong, local control on regional climate. We compare the areas affected by (1) the southern, Paranan (60 °W, 25–40 °S) and (2) northern, Amazonia (Brazil, Peru, Bolivia) regions of the seaway. In the Paranan region, evaporation and humidity increase but temperature decreases (Fig. 4G), and precipitation rates remain very low (Figs. 2C and 4C). In the Amazonia region, summer surface temperatures (Fig. 4G) are higher in the presence of a seaway. Higher relative and specific humidity over the seaway results in an increase in precipitation downwind in the northern and central Andes of up to 4–6 mm/day (Fig. 4C).

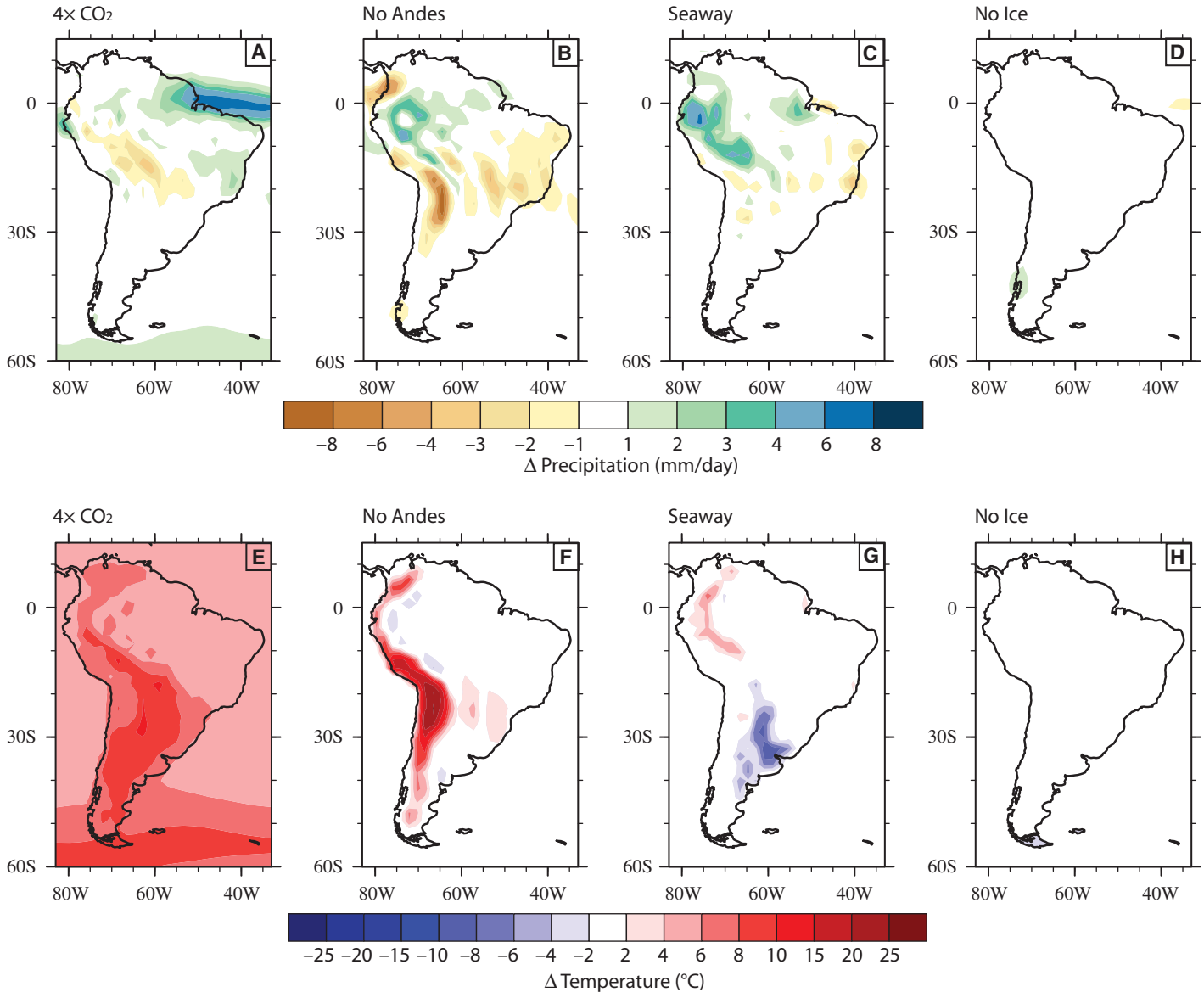

Figure 4. Austral summer climatology. Simulated summer precipitation (mm/day) (A–D) and temperature (°C) (E–H) difference between simulation and control (simulation minus control; see Figs. 2B and 2C) for (A and E) 4× CO_2; (B and F) No Andes; (C and G) Seaway; (D and H) No Ice. Note that the contour intervals change at 6 mm/day and 10 °C in the precipitation and temperature plots, respectively. Although isotopes are different in the freshwater and marine seaway runs, the climate is identical.

The effects of the seaway and the resultant climatic changes on $\delta^{18}O_{prec}$ depend on the $\delta^{18}O_{seaway}$. Two experiments, SW_{marine} and $SW_{freshwater}$, have a $\delta^{18}O_{seaway}$ of ~–1‰ and –6‰, respectively. In the SW_{marine} experiment (Figs. 5C and 5H), the $\delta^{18}O_{prec}$ south of 25 °S (Paranan) is up to 4‰ less negative than the control simulation. North of 25 °S (Amazonia), $\delta^{18}O_{prec}$ is more negative than the control simulation by 2–4‰. Maximum depletion occurs in the northern Andes and the Amazon basin. In contrast, the $SW_{freshwater}$ experiment results in more negative $\delta^{18}O_{prec}$ throughout the continent (Figs. 5D and 5I). Maximum depletion occurs in the northern Andes, where the lowest values are between –22‰ and –20‰, 6–8‰ more negative than the control simulation.

Source and amount effects are responsible for changes in $\delta^{18}O_{prec}$ in the presence of a seaway. In the Paranan region, where simulated average precipitation rates are <1 mm/day, the isotopic composition of the seaway dictates the direction of change in $\delta^{18}O_{prec}$. The $\delta^{18}O_{prec}$ will shift in the direction of the $\delta^{18}O_{seaway}$. For example, in the SW_{marine} case, $\delta^{18}O_{prec}$ becomes more negative. In the Amazonian region, the seaway drives an increase in precipitation and therefore rainout effects, lowering the $\delta^{18}O_{prec}$. The $\delta^{18}O_{seaway}$ determines the magnitude of $\delta^{18}O_{prec}$ depletion relative to the control. A more depleted seaway ($SW_{freshwater}$) causes a more negative $\delta^{18}O_{prec}$ (Figs. 5H and 5I). Temperature changes (Fig. 4G) may also alter the $\delta^{18}O_{prec}$ but are not the dominant control because the simulated temperature changes are expected to have the opposite effect on $\delta^{18}O_{prec}$ than those simulated.

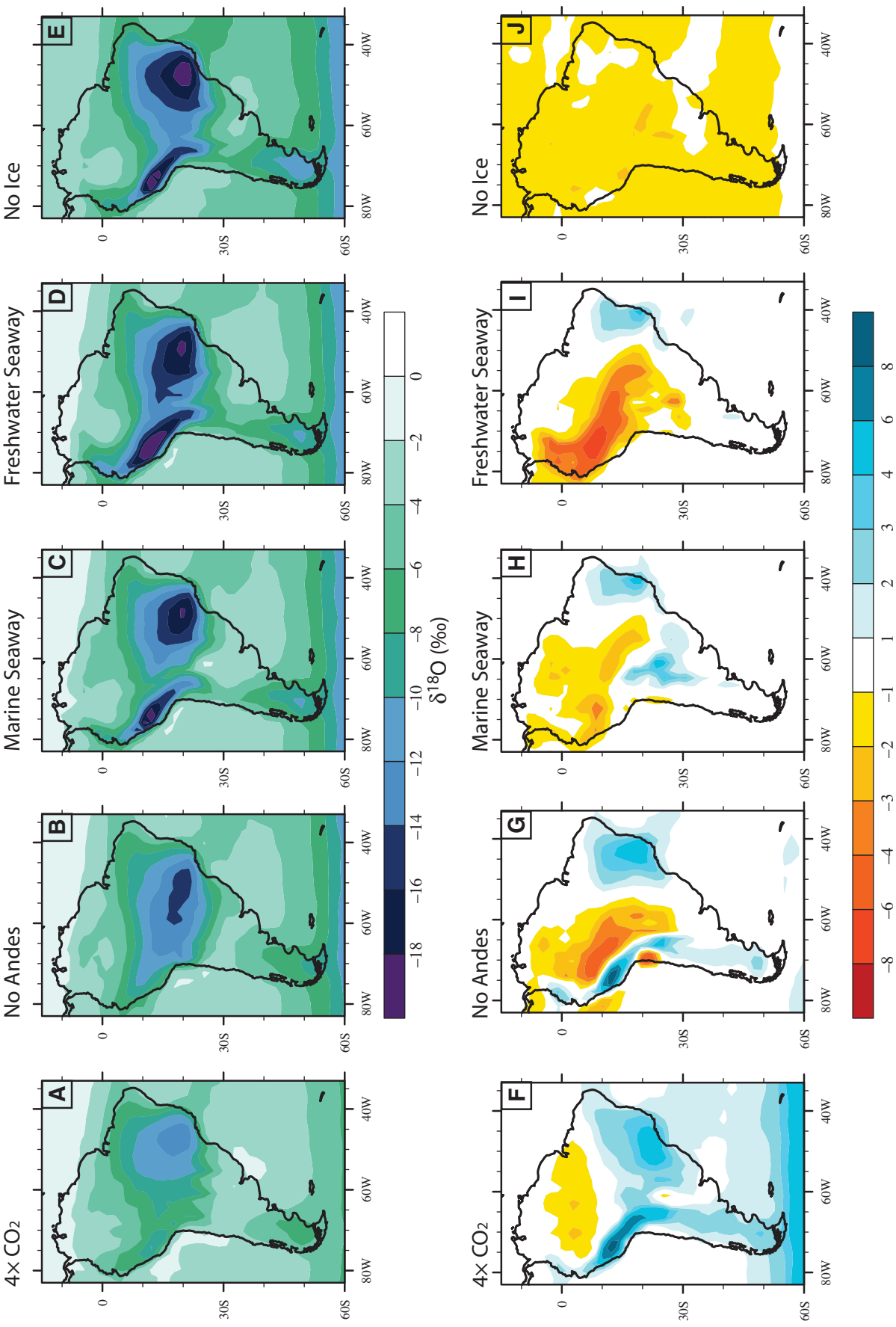

Figure 5. Austral summer $\delta^{18}O_{prec}$. (A–E) Simulated amount-weighted summer $\delta^{18}O_{prec}$ (‰) predicted by GENESIS with (A) 4× CO_2; (B) No Andes; (C) SW_{marine}, a seaway (see Fig. 2A) with a marine, Atlantic-like, isotopic composition; (D) $SW_{freshwater}$, a seaway with freshwater (–6‰) composition; and (E) No Ice, Ocean–No Antarctic ice sheet ($\delta^{18}O_{ocean}$ = modern $\delta^{18}O_{ocean}$ – 1.2‰). (F–J) Summer $\delta^{18}O_{prec}$ difference (simulation minus control) between the sensitivity simulation and the control run (Fig. 2D) for the simulations in (A–E). Note that the contour interval changes at 4‰.

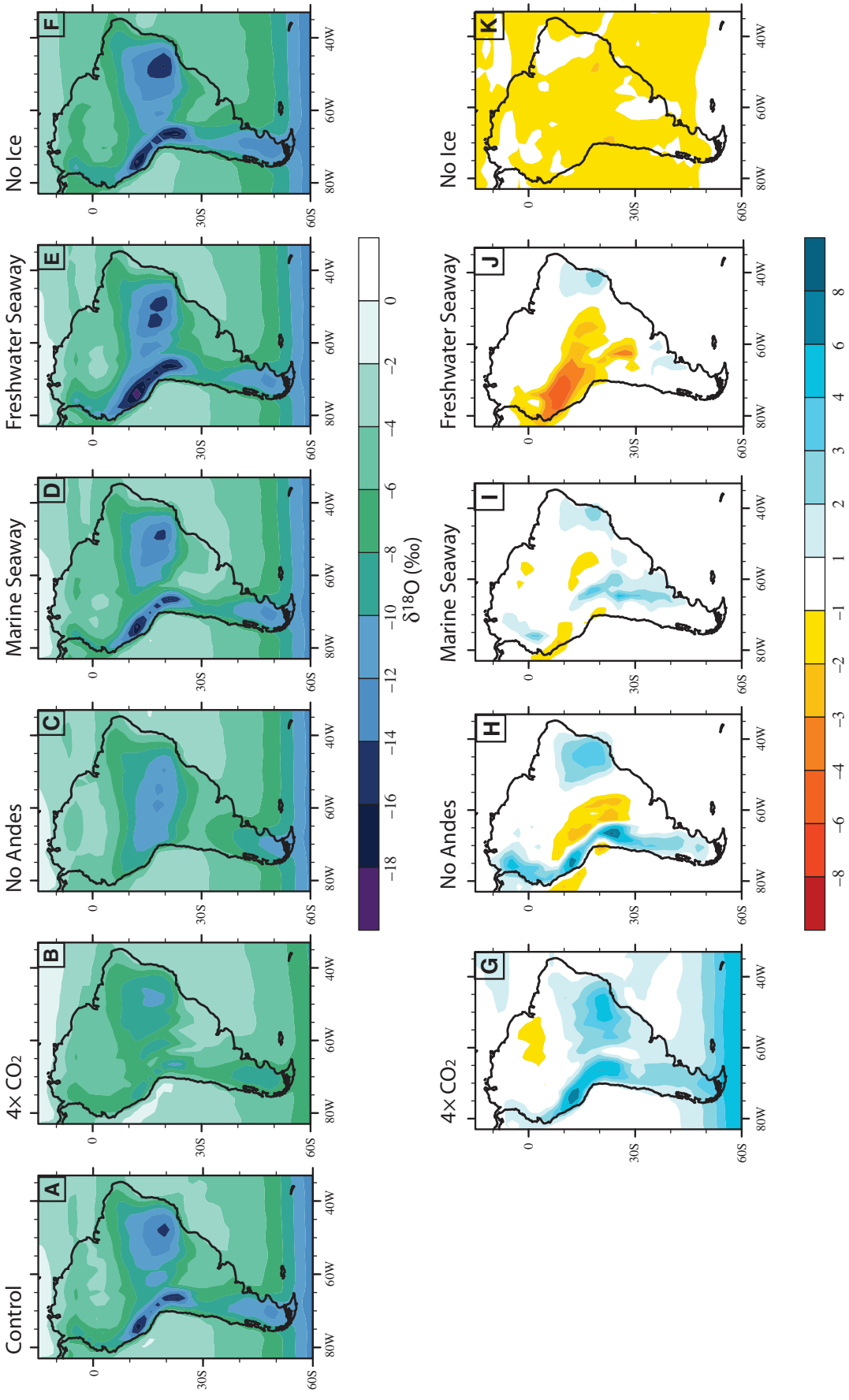

Figure 6. Mean annual $\delta^{18}O_{prec}$, (A–F) Simulated amount–weighted mean annual $\delta^{18}O_{prec}$ (‰) predicted by GENESIS with (A) modern conditions; (B) 4× CO_2; (C) No Andes; (D) SW_{marine}, a seaway (see Fig. 2A) with a marine, Atlantic-like, isotopic composition; (E) $SW_{freshwater}$, a seaway with freshwater (–6‰) composition; and (F) No Ice, Ocean–No Antarctic ice sheet ($\delta^{18}O_{ocean}$ = modern $\delta^{18}O_{ocean}$ – 1.2‰). (G–K) Mean annual $\delta^{18}O_{prec}$ difference (simulation minus control) between the sensitivity simulation and the control run (Fig. 6A) for the simulations in (B–F). Note that the contour interval changes at 4‰.

Antarctic Ice Sheet Effects on $\delta^{18}O_{prec}$

The removal of the ice sheet results in a global MAT rise of 0.9 °C from 12.6 °C to 13.5 °C. However, temperature increases predominantly occur south of 45 °S and are not observed in the summer average over South America (Fig. 4H). Precipitation rates change by 1–2 mm/day in a few isolated regions (e.g., 75 °W; 40 °S, Fig. 4D).

The physical removal of the ice sheet (NoIce_modOcean experiment) results in small regions that are 0–2‰ more negative than the control simulation (e.g., 0 °S, 65 °W; Figs. DR1E and DR1J [see footnote 1]). The addition of isotopically light meltwater to the oceans results in precipitation that is isotopically more depleted by a further ~1.2‰ (NoIce experiment, Fig. 5E). In the model, the change in $\delta^{18}O_{ocean}$ therefore causes a change in $\delta^{18}O_{prec}$ of the same magnitude and is the dominant mechanism by which Antarctic ice formation alters South American $\delta^{18}O_{prec}$. The maximum impact of the ice sheet on $\delta^{18}O_{prec}$ is ~2–3‰, but the impact is generally <2‰ (Fig. 5J).

Time-Specific Paleoclimate Scenarios

Interpretation of $\delta^{18}O_{prec}$ records requires quantifying the combined effects of more than one control. Here we explore two time scenarios: (1) the late Eocene (Figs. 7A–7D), when Andean uplift began, and (2) the middle Miocene (Figs. 7E– 7H), preceding and during the formation of many of the central Andean $\delta^{18}O_{prec}$ records.

Late Eocene, ca. 40 Ma

The late Eocene scenario includes a low-elevation Andes, 4×CO_2, no Antarctic ice sheet or interior seaway, and a $\delta^{18}O_{ocean}$ corrected for ice-sheet volume. Maximum temperatures of >40 °C occur between 20 °S and 30 °S in the Eocene simulation, which is >10 °C warmer than the present-day foreland and >30 °C warmer than the present-day (control simulation) high Andes at this latitude (Figs. 2B and 7D). Precipitation rates are reduced in the central and northern Andes as a result of the removal of an orographic barrier, while elevated CO_2 and low Andean elevation lead to increased precipitation in the Amazon and equatorial Atlantic (Figs. 2C and 7C).

The middle Eocene $\delta^{18}O_{prec}$ pattern (Fig. 7A) is significantly different than the modern (Fig. 2D). A single strong $\delta^{18}O_{prec}$ minimum occurs in central South America, with a weaker minimum in the southern Andes. In the Eocene simulation, precipitation is isotopically less depleted by >8‰ along the Andean range and 6–8‰ in eastern Brazil (Fig. 7B). Maximum differences between the Eocene and control simulation occur in the northern central Andes and western Amazon. The more negative $\delta^{18}O_{prec}$ in the Amazon is associated with greater upwind precipitation rates (Figs. 2C and 7C). Higher temperatures (Figs. 2B and 7D) and reduced rainfall rates (Figs. 2C and 7C) result in less negative $\delta^{18}O_{prec}$ values elsewhere and particularly on the eastern central Andean flanks.

Middle Miocene, ca. 15 Ma

The middle Miocene experiment is performed using half Andean elevation and 2×CO_2 (Table 1). Simulated middle Miocene temperatures in the Altiplano region are 20–25 °C, and precipitation rates are 3–11 mm/day (Figs. 7G and 7H), 10–15 °C cooler on the Altiplano, and 6 mm/day drier on the eastern flanks than the control simulation (Figs. 2B, 2C, 7G, and 7H). In the Miocene simulation, $\delta^{18}O_{prec}$ is less negative everywhere in the Andes (by 2–8‰) and in eastern Brazil than the control simulation; but in the Amazon basin, $\delta^{18}O_{prec}$ is more negative. The maximum decrease in $\delta^{18}O_{prec}$ occurs in the southern Altiplano (Fig. 7F).

Cenozoic $\delta^{18}O_{prec}$ Patterns in South America

Combining the boundary conditions in these time-appropriate scenarios allows us to make estimations of past climate and $\delta^{18}O_{prec}$ patterns. Based on the modern, Miocene, and Eocene simulations, we expect that $\delta^{18}O_{prec}$ had lower spatial gradients and variability in the past (Figs. 2D, 7A, and 7E). For example, the extreme low values in the central and southern Andes and in eastern Brazil (45 °W, 20 °S) that are present in the control simulation are not as low in the Miocene scenario and are weak or not present in the Eocene scenario. The Miocene $\delta^{18}O_{prec}$ pattern is similar to modern but shifted toward less negative values with lower spatial gradients. At half the modern elevation, the Andes are still capable of modifying the regional climate and $\delta^{18}O_{prec}$. The Eocene $\delta^{18}O_{prec}$ pattern is simple with $\delta^{18}O_{prec}$ decreasing away from the coasts and toward higher latitudes.

In both scenarios, changes in temperature and precipitation patterns are consistent with the sensitivity experiments of the individual parameters. However, the total change in $\delta^{18}O_{prec}$ in the Eocene scenario (Fig. 7B) is less than that expected from sensitivity experiments in which only Andean elevation, CO_2, or $\delta^{18}O_{ocean}$ are changed (Figs. 5F, 5G, and 5J). This discrepancy is mainly due to $\delta^{18}O_{prec}$ responding differently to increasing CO_2 in the absence of the Andes. A strengthening of the Chaco Low, a low-pressure system in central South America, and changes in moisture source with increasing CO_2 result in precipitation that is isotopically more depleted at low Andean elevations despite an increase in temperature.

IMPACTS OF CENOZOIC GLOBAL CLIMATE AND REGIONAL GEOGRAPHY CHANGES ON SOUTH AMERICAN CLIMATE AND $\delta^{18}O_{prec}$ RECORDS

The simulations presented here show that global and regional climatic change can exert a significant influence on $\delta^{18}O_{prec}$. Here we compare the simulation results with existing climate and stable isotope records.

Impact of Global Climate and Regional Geography Changes on South American Climate

The climate of South America is significantly altered by a rise in CO_2, a change in Andean elevation, and the presence of an inland seaway (Figs. 4A–4C and 4E–4G) but less so by the presence or absence of the Antarctic ice sheet (Figs. 4D and 4H). Although spatially variable, temperatures increase everywhere in response to an increase in CO_2, whereas only local temperature changes occur in response to increasing Andean elevations and seaway incursions. An increase from no Andean elevation to full Andean elevation causes the greatest changes in surface temperature (up to 25 °C in the central Andes, Fig. 4F), but temperature changes under high (4×) CO_2 conditions are significant in comparison (10 °C, Fig. 4E). Predicted temperature changes in the presence of a seaway are mainly limited to the seaway and do not extend to high elevations (Fig. 4G). Given this, surface-temperature records from multiple locations could help to distinguish between these factors. For example, a drop in temperature of 10 °C on the Andean plateau could represent an elevation increase of around half (~2000 m), or a doubling of CO_2 and an elevation increase of one third. The former would not be accompanied by temperature changes in the foreland, while the latter would show an increase in temperature of ~3 °C in the foreland. This example highlights how sampling strategies could not only quantify the paleoclimate, but also help delineate between different mechanisms of climate change.

The seaway, Andean elevation, and, to a lesser extent, CO_2 levels, are capable of causing large changes in the magnitude of precipitation rates in the northern Andes (Figs. 4A–4C). Precipitation rates in the central Andes are modified primarily by Andean elevation; an increase in elevation causes an increase in precipitation on the eastern flanks. In the southern Andes, atmospheric CO_2 is the dominant control on precipitation, particularly in the winter months (Fig. DR2 [see footnote 1]), in addition to some changes in response to elevation increase.

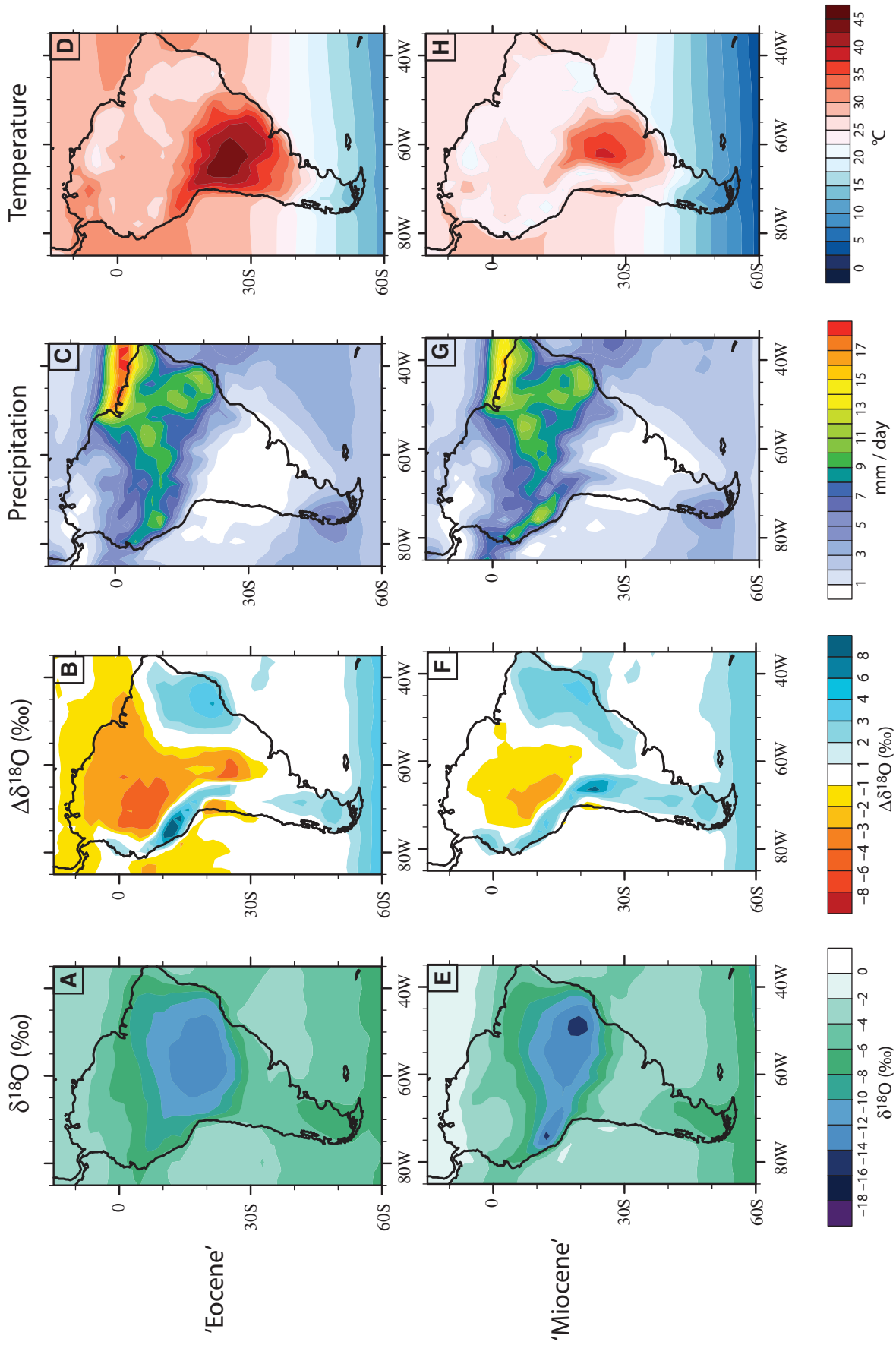

Figure 7. Climatology and $\delta^{18}O_{prec}$ for Eocene and Miocene scenarios. Simulated austral summer amount-weighted $\delta^{18}O_{prec}$, difference in $\delta^{18}O_{prec}$, precipitation (mm/day), and temperature (°C) for the late Eocene (A–D) and middle Miocene (E–H) simulations. Difference in $\delta^{18}O_{prec}$ (B and F) is simulation minus control (Fig. 2D). The Eocene simulation has No Andean elevation, 4× CO_2, and No Antarctic ice sheet ($\delta^{18}O_{ocean}$ = modern $\delta^{18}O_{ocean}$ − 1.2‰). The Miocene simulation has half Andean elevation, 2× CO_2 and a modern ice sheet and $\delta^{18}O_{ocean}$. Neither simulation includes a seaway. Note that the contour level changes in $\Delta\delta^{18}O_{prec}$.

Precipitation rates in the Amazon region and eastern Brazil depend on CO_2 levels, Andean elevation, and the seaway.

Impact of Global Climate and Regional Geography Changes on South American $\delta^{18}O_{carb}$ Records

Existing South American Stable Isotope Records

Simulation of $\delta^{18}O_{prec}$ can improve interpretations of $\delta^{18}O_{prec}$ records by showing the relative importance of different controls on $\delta^{18}O_{prec}$ for a given region. A brief summary of currently available records of Cenozoic South American $\delta^{18}O_{prec}$, including data from soil carbonates, lacustrine carbonates, and biogenic apatite from fossil mammal teeth, is as follows (see also Fig. 8):

(1) In the northern Andes, few carbonate stable isotope records exist because the climate is wet and not conducive for soil carbonate formation. An exception to this is a recent study by Giovanni et al. (2010), who report lacustrine carbonate data from the Cordillera Blanca, Peru; these carbonates were deposited <5.4 Ma (Fig. 8A). The $\delta^{18}O_{carb}$ sample values range from –13.2‰ to –17.8‰, indicating that $\delta^{18}O_{prec}$ was strongly depleted and suggesting that high elevations had been attained in this region by ca. 5 Ma.

(2) Central Andean climate is more conducive to carbonate formation, and data are available from the plateau and both flanks. Palustrine and pedogenic carbonates from the northern Altiplano (Fig. 8B) record a decrease in $\delta^{18}O_{carb}$ from between –6‰ and –8‰ at ca. 28 Ma to between –10‰ and –16‰ at ca. 6 Ma (Garzione et al., 2008; Garzione et al., 2006). The late Miocene part of this record indicates a 3–4‰ decrease in mean $\delta^{18}O_{mw}$ between 10 and 6 Ma (Garzione et al., 2006), when converted from $\delta^{18}O_{carb}$ using paleotemperatures extracted from the same records using Δ47 clumped isotope paleothermometry (Ghosh et al., 2006). Fossil mammal teeth from the northern Altiplano show a decrease of ~10‰ in $\delta^{18}O_{mw}$ from ca, 26 Ma to 10–8 Ma (Fig. 8C, Bershaw et al., 2010). The $\delta^{18}O_{carb}$ from the eastern Andean flanks record a decrease of ~5‰ between 12.4 and 8.5 Ma and then an increase of ~4‰ by 7.5 Ma (Fig. 8D, Mulch et al., 2010). This pattern was attributed to Andean uplift and the initiation of a wetter and more seasonal climate (Mulch et al., 2010). A second record from the eastern flanks, but at lower modern elevations, shows fluctuations of $\delta^{18}O_{carb}$ between –14‰ and –6‰, prior to 7 Ma (Uba et al., 2009). The less negative $\delta^{18}O_{carb}$ values are from facies that are interpreted as marine inland seaway deposits. Palustrine and lacustrine carbonates from the Atacama Desert document a ~5‰ increase in $\delta^{18}O_{carb}$ between 12 and 6 Ma, which is attributed to increased aridity due to the creation of an orographic barrier when Andean heights are >2 km (Fig. 8E, Rech et al., 2010). To the south in northwest Argentina, Kleinert and Strecker (2001) identify an increase in pedogenic $\delta^{18}O_{carb}$ from between –11‰ and –8‰, 12–9 Ma, to ~–6.5‰ by 7–3 Ma and a further increase to between –5.5‰ and –1.5‰ during the Plio-Pleistocene (Fig. 8F). The $\delta^{18}O_{carb}$ increase was attributed to increasing evaporation in a more seasonal and drier climate, despite expected depletion due to the development of a rain shadow. Nearby, Latorre et al. (1997) document an increase in $\delta^{18}O_{carb}$ of 4‰ between 9 and 3.5 Ma (Fig. 8G), which they suggested may be due to an increase in seasonality and evaporation, possibly on a global scale.

(3) Finally, in the eastern foreland of the Patagonian Andes, a decrease of 2‰ and an increase in variability is observed in pedogenic $\delta^{18}O_{carb}$ at ca. 16.5 Ma (Fig. 8H, Blisniuk et al., 2005). This change is attributed to rain-shadow development that is slightly masked by increased evaporation, both of which are a consequence of Andean uplift.

Evaluation of $\delta^{18}O_{prec}$ Records Based on Simulation Results

This wealth of $\delta^{18}O_{prec}$ data records provides valuable constraints on the tectonic and climatic evolution of South America. However, the majority of these records are currently interpreted in terms of local- and regional-scale processes and do not account for either global climate change or a seaway incursion. In some cases, local controls may dominate the signal; however, discounting regional change may lead to an over- or under-estimation of the magnitude of change in the dominant control.

The $\delta^{18}O$ composition of carbonates is dependent on the local evaporation rate and soil temperature during carbonate precipitation as well as the $\delta^{18}O$ composition of the local meteoric water ($\delta^{18}O_{mw}$). Increasing evaporation rates and decreasing soil temperatures drive increases in $\delta^{18}O_{carb}$ (Kim and Oneil, 1997; Quade et al., 1989). Distinguishing these three different controls is complex but is possible with (1) additional constraints on temperature, (2) sedimentological evidence of increasing aridity and/or humidity as an indicator of changing evaporation rates, and (3) prediction of $\delta^{18}O_{prec}$ based on climate models and known climatic constraints. Climate models enable us to estimate both changes in surface temperature and $\delta^{18}O_{prec}$ for a given change in boundary conditions. Predictions of both $\delta^{18}O_{prec}$ and temperature effects on carbonate formation can then be combined when examining $\delta^{18}O_{carb}$ records. Assuming that a decrease in surface temperature causes an increase in $\delta^{18}O_{carb}$ of ~0.12‰/°C (Kim and Oneil, 1997), a temperature increase of ~10 °C would increase $\delta^{18}O_{carb}$ by 1.2‰. Because GENESIS simulates surface temperature and not temperature at the depth of carbonate formation, these values are an approximation but help to determine the relative importance of temperature and $\delta^{18}O_{prec}$ changes. For many of the boundary conditions presented here, predicted temperature effects are small compared to changes in $\delta^{18}O_{prec}$. Exceptions to this are the climatic responses to increasing elevation and decreasing CO_2 at low elevations. On the Andean Plateau, increasing elevation from low to full Andean elevation results in a temperature increase of 20–25 °C and a decrease in $\delta^{18}O_{prec}$ of 3–6‰, leading to a net decrease of ~0–3.5‰ in $\delta^{18}O_{carb}$. Decreasing CO_2 from 4× to 1× PIL results in a temperature decrease of 6–8 °C, a $\delta^{18}O_{prec}$ decrease of 4–6‰ and therefore a decrease in $\delta^{18}O_{carb}$ of ~3–5‰. The seaway and ice sheet do not affect surface temperatures (Figs. 4G and 4H).

The very negative ca. 5 Ma $\delta^{18}O_{carb}$ found in the northern Andes (Fig. 8A, Giovanni et al., 2010) has been attributed to high Andean elevations at that time. Our results show that the presence of a freshwater seaway could lower $\delta^{18}O_{prec}$ by >4‰ in this region. However, the seaway had retreated by ca. 7 Ma (Hoorn et al., 2010), and it is therefore unlikely that a seaway contributed to these low $\delta^{18}O_{carb}$ observations. Increasing Andean elevation from half to modern elevation leads to a simulated decrease in $\delta^{18}O_{prec}$ of only 2–3‰ in the northern Andes (Fig. DR1F), which is less than the spread of values recorded over a short period of time. We suggest that this record is consistent with Andean elevations that were within ~2000 m of the modern elevation by ca. 5 Ma.

Andean Plateau $\delta^{18}O_{carb}$ records indicate a decrease of ~1–2‰ in $\delta^{18}O_{carb}$, and an increase in $\delta^{18}O_{carb}$ variability between 10 and 6 Ma (Garzione et al., 2006). Ehlers and Poulsen (2009) and Poulsen et al. (2010) demonstrate that this record is consistent with increasing Andean uplift accompanied by a decrease in surface temperature and increases in convective precipitation on the Andean flanks. However, decreasing CO_2 could also have contributed to decreasing $\delta^{18}O_{carb}$, reducing the amount of surface uplift required to produce the same $\delta^{18}O_{carb}$ signal. The $\delta^{18}O_{prec}$ is lowered by >3‰ on the Altiplano when CO_2 decreases from 2× to 1× PIL (Fig. DR1G [see footnote 1]). The CO_2 levels have not exceeded 2× PIL since 10 Ma (Demicco et al., 2003; Pagani et al., 2005; Pearson and Palmer, 2000), but even a 1.5‰ CO_2-driven decrease in $\delta^{18}O_{prec}$

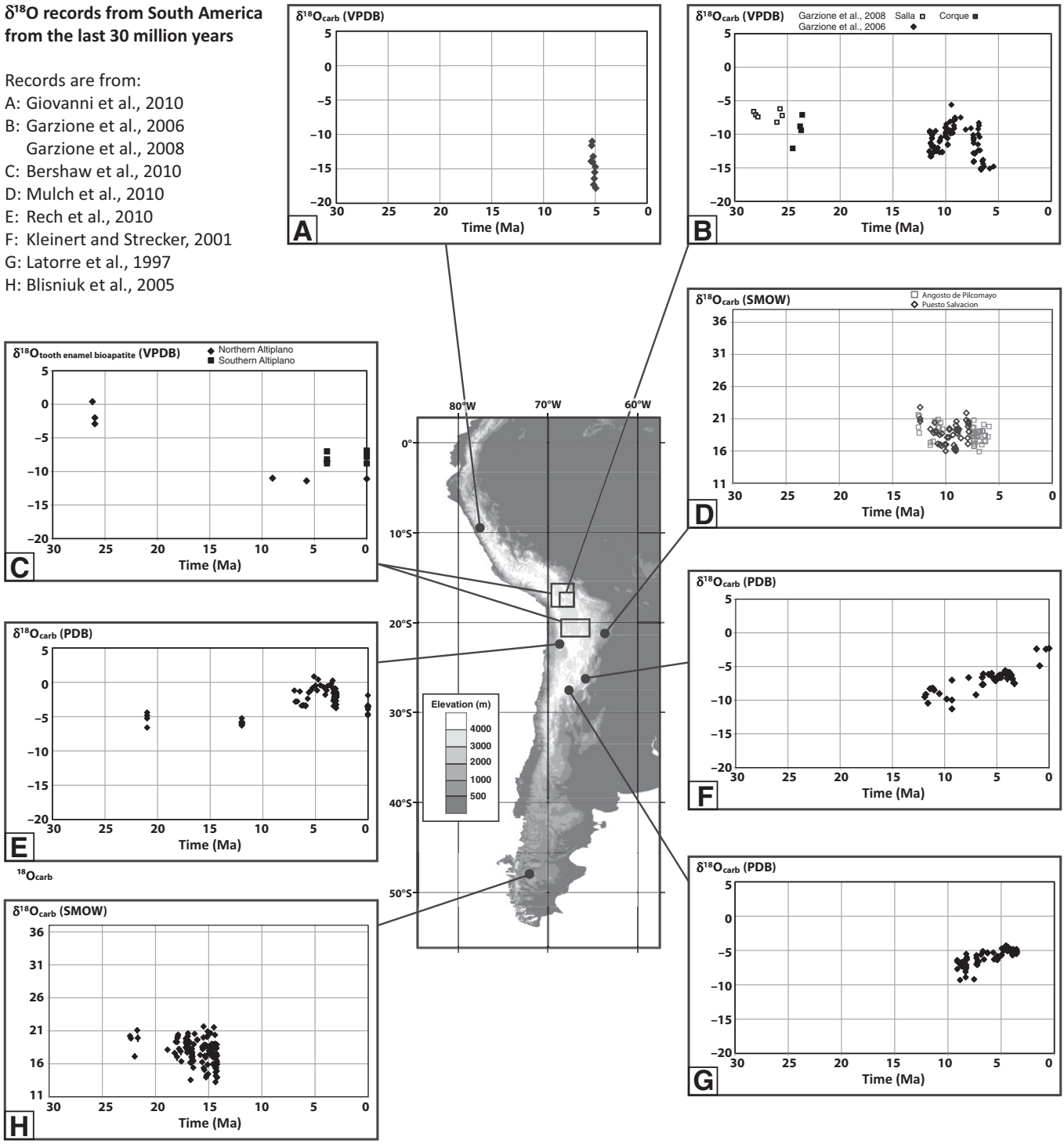

Figure 8. The $\delta^{18}O$ records from South America (30 Ma–present). Records presented here are derived from soil or lake carbonates unless otherwise stated. Circles and boxes indicate the location of sample sites within South America. (A) Giovanni et al. (2010); (B) Garzione et al. (2006) and Garzione et al. (2008); (C) Bershaw et al. (2010): $\delta^{18}O$ of carbonate component of bioapatite in fossil mammal tooth enamel; (D) Mulch et al. (2010); (E) Rech et al. (2010); (F) Kleinert and Strecker (2001); (G) Latorre et al. (1997); and (H) Blisniuk et al. (2005). In order to plot the data on the same plots, some of the data have been assigned ages based on the age constraints and sedimentation rate estimates given in the original papers (Blisniuk et al., 2005; Giovanni et al., 2010; Mulch et al., 2010; Rech et al., 2010). Where possible, constant sedimentation rates are assumed based on dated horizons within the observed stratigraphy. The record presented in Giovanni et al. (2010) has only one age constraint of 5.45 Ma at the base of the section. For ease of viewing, we assume that the first sample is 5.45 Ma, and consecutive measurements are at 0.05 m.y. intervals. Data sets reported against different $\delta^{18}O$ standards have been plotted so that the y-axes correspond to approximately equivalent $\delta^{18}O_{carb}$ values. PDB—PeeDee belemnite; VPDB—Vienna PeeDee belemnite; SMOW—standard mean ocean water.

would result in underestimates of paleoelevation by ~500–750 m. Conversely, the presence of a freshwater seaway from 15 to 7 Ma, but not after ca. 7 Ma, would mask an increase in elevation between 10 and 6 Ma.

The ~30-m.y. isotopic record of mammal teeth from the Altiplano indicates a decrease in $\delta^{18}O_{mw}$ of ~10‰ between 26 Ma and 10 Ma (Bershaw et al., 2010). Due to lack of data, it is impossible to determine whether the transition from 26 to 10 Ma was gradual or punctuated. Increasing elevation and decreasing CO_2 levels are capable of decreasing $\delta^{18}O_{mw}$. However, a decrease of 10‰ exceeds the isotopic response to any one control, or the combination of controls in the Miocene and Eocene scenarios. Possible reasons for this discrepancy include regional changes, e.g., ocean circulation, that are not accounted for in our experiments or higher evaporation rates at 26 Ma. Another possibility is that a seaway lowered $\delta^{18}O_{prec}$ at ca. 10 Ma, contributing to the overall decrease from 26 to 10 Ma. This decrease in $\delta^{18}O_{mw}$ is consistent with the decrease in $\delta^{18}O_{carb}$ observed over a similar time period (Fig. 8B, Garzione et al., 2008), although the observed decrease in $\delta^{18}O_{carb}$ is smaller possibly due to changes in temperature or evaporation rates.

The late Miocene decreasing trends in $\delta^{18}O_{carb}$ on the Altiplano contrast with records from the western and eastern Andean flanks, which indicate increases of between 5‰ and 8‰ since ca. 11 Ma (Figs. 8E–8G; Kleinert and Strecker, 2001; Latorre et al., 1997; Rech et al., 2010). These $\delta^{18}O_{carb}$ increases are consistent with decreasing local surface temperatures, increasing evaporation rates, and changing seasonality. Changing seasonality could alter $\delta^{18}O_{carb}$ by changing the aridity and $\delta^{18}O_{prec}$ during the season of carbonate formation. This increase is also consistent with increasing Andean elevation. On the eastern flanks, our simulation results show that as Andean elevation increases, $\delta^{18}O_{prec}$ in the adjacent foreland increases. This is because as Andean plateau elevations increase, the strengthening South American low-level jet transports enriched water vapor farther across the Amazon basin (Poulsen et al., 2010). Additionally, simulated evaporation rates on the eastern flanks increase with increasing elevation. However, precise identification of the locations of $\delta^{18}O_{carb}$ increase relative to $\delta^{18}O_{prec}$ increase would require simulations at a higher resolution than those presented here, and this mechanism does not explain the contemporaneous increase in $\delta^{18}O_{carb}$ on the western flanks (Fig. 8E). Increasing ice-sheet size may have contributed ~1‰ to increasing $\delta^{18}O_{prec}$ since 10 Ma. Retreat of the seaway occurred before ca. 7 Ma and is therefore unlikely to have contributed to increases in $\delta^{18}O_{carb}$ that extend throughout the past 10 Ma.

However, the seaway could have contributed to the negative $\delta^{18}O_{carb}$ excursion observed in the eastern Bolivian Andes by Mulch et al. (2010, Fig. 8D) between 10 and 7 Ma. Although an Amazonia seaway was present from ca. 24 to 7 Ma, the extent of the seaway fluctuated through time (Hovikoski et al., 2007; Uba et al., 2009). Constraining the timing, extent, and isotopic composition of the seaway is a critical step in determining the influence of the seaway on $\delta^{18}O_{carb}$ records. Results show that the seaway has the potential to drive a decrease in $\delta^{18}O_{carb}$ at this location, but at this time it is not possible to determine how important the seaway was to these $\delta^{18}O_{carb}$ records. It is likely that the seaway did influence the $\delta^{18}O_{carb}$ records, but it may have contributed to the observed variability rather than the long-term trends.

When examining $\delta^{18}O_{carb}$ records from the southern Andes, it is more appropriate to use the mean annual $\delta^{18}O_{prec}$ results because DJF is not the dominant rainfall season there. CO_2 exerts the strongest control on $\delta^{18}O_{prec}$ (Figs. 7F–7J), and we suggest that the contribution of CO_2 to $\delta^{18}O_{carb}$ from this region (Fig. 8H) has previously been underestimated. For example, fluctuating CO_2 levels associated with the middle Miocene climatic optimum (Kurschner et al., 2008; Sheldon, 2006) may have at least contributed to the high variability seen in the $\delta^{18}O_{carb}$ record, if not the longer term trends as well.

This review of the available $\delta^{18}O_{carb}$ records from South America indicates that Andean uplift likely played a dominant role in determining $\delta^{18}O_{prec}$ during the past 15 Ma. Uplift of the Andes alters $\delta^{18}O_{prec}$ both as a direct result of lower temperatures at higher elevation and also through modification of regional circulation patterns. However, CO_2 levels and an inland seaway also contributed to $\delta^{18}O_{prec}$. Discounting these latter effects could lead to misinterpretations of paleoelevation and paleoclimate. Key uncertainties in making more detailed predictions about observed $\delta^{18}O_{carb}$ records using simulation results include knowledge of CO_2 levels, timing of Andean uplift, and the timing and isotopic composition of seaway incursions. Terrestrial temperature records and good spatial distribution of contemporaneous $\delta^{18}O_{carb}$ records are potential avenues by which to improve constraints on the relevant controls for a particular time period.

Implications for Paleoaltimetry Data Interpretation

Stable isotope paleoaltimetry techniques use modern isotopic lapse rates to infer changes in elevation from records of $\delta^{18}O_{prec}$. Paleoelevation estimates from the Andes place an important constraint on plateau formation mechanisms (Barnes and Ehlers, 2009; Garzione et al., 2006). Our results show that changes in global and regional climate can complicate the extraction of paleoelevation estimates from the $\delta^{18}O_{carb}$ record. Specifically, the model results show that an underestimate of paleoelevation would be made from carbonates that formed at elevated CO_2 levels (see also Poulsen and Jeffery, 2011) and estimates that do not account for climatic change caused by Andean surface uplift. In contrast, $\delta^{18}O_{ocean}$ changes associated with lower ice volumes would lead to paleoelevation estimates that are too high. Impacts of the seaway on paleoaltimetry depend on the timing and composition of the seaway; if the seaway were present at the time of carbonate formation, paleoelevations would again be overestimated, possibly by as much as ~1000 m. For example, a shift in $\delta^{18}O_{mw}$ of 4‰ would be interpreted as an elevation change of 1400 m based on a modern global average lapse rate of 2.8‰/km (Poage and Chamberlain, 2001). We note, however, that this number is an approximation because lapse rates have been documented to be temporally and spatially variable (Poulsen et al., 2010). A local Andean lapse rate of 2.1‰/km (Gonfiantini et al., 2001) would yield an estimated elevation change of 1900 m for a $\delta^{18}O_{mw}$ shift of 4‰, approximately half of the modern Andean Plateau elevation. At least half of such a 4‰ shift in $\delta^{18}O_{mw}$ could be driven by changing CO_2 levels or an inland seaway incursion. If this were the case, paleoelevation estimates would be in error by ~700–1000 m or more.

Caveats

Like all modeling studies, this study has limitations that should be considered in evaluating the results. In comparison to most paleoclimate studies, we have used a fairly high-resolution global climate model. Nonetheless, spectral truncation reduces the maximum elevation of high, narrow mountain ranges such as the Andes, which reduces the maximum orographic precipitation and raises minimum temperatures. As a result of using an older topographic data set, the simulated topography in the southern Andes is slightly too low, which may reduce the magnitude of simulated change in $\delta^{18}O_{prec}$ when the Andes are lowered. However, due to the spectral truncation of narrow topography, a higher elevation in the initial data set is unlikely to make a large difference. However, the general patterns of wet or dry and cold or warm regions are well represented in the model, as are the $\delta^{18}O_{prec}$ patterns. Our use of a slab-ocean model prohibits the simulation of ocean-surface currents and longitudinal variations in sea-surface

temperatures. The distribution of sea-surface temperatures is known to be important to modern South American climate. For example, the Humboldt current promotes hyperaridity in the Atacama Desert (Hartley, 2003; Houston and Hartley, 2003), and El Niño–La Niña Southern Oscillation governs interannnual variability (Ropelewski and Halpert, 1987). A more realistic sea surface temperature (SST) distribution improves the simulated modern climate using GENESIS and is likely to improve the simulated $\delta^{18}O_{prec}$ distribution as well. Future simulations incorporating an ocean circulation model will help to reduce this uncertainty. The vegetation in our simulations is prescribed as modern. Important climatic processes such as moisture recycling in the Amazon region depend on vegetation properties. Given the amount of climatic change simulated, it is likely that the vegetation patterns have also changed. Such vegetation changes are unlikely to have large direct impacts on $\delta^{18}O_{prec}$ but may influence the climate, and thus indirectly $\delta^{18}O_{prec}$. Finally, uncertainties in the paleoclimate record of the boundary conditions and their implementation in the model lead to uncertainties in the interpretation of $\delta^{18}O_{carb}$. In particular, improved knowledge of past atmospheric CO_2 levels and the nature and timing of the inland seaway would provide better constraints on potential causes of $\delta^{18}O_{carb}$ shifts.

CONCLUSIONS

Our results indicate that both global and regional factors have significantly modified the climate and $\delta^{18}O_{prec}$ of South America during the Cenozoic. Precipitation rates are modified by changes in elevation, and higher precipitation rates are caused by the presence of the South American inland seaway in the mid to late Miocene.

$\delta^{18}O_{prec}$ is sensitive to Cenozoic climate and environmental change. In particular, $\delta^{18}O_{prec}$ is expected to have decreased over most of the continent through the Cenozoic, except in the Amazon basin, due to increasing Andean elevation and decreasing atmospheric CO_2. This trend is partially counteracted by an increase in $\delta^{18}O_{ocean}$ as a consequence of ice-sheet formation. An excursion toward more negative $\delta^{18}O_{prec}$ is predicted during the mid-late Miocene when an inland seaway was present. Uncertainty in the timing, extent, and isotopic composition of the South American inland seaway limits our ability to predict the impact of the seaway on $\delta^{18}O_{carb}$ records. The $\delta^{18}O_{prec}$ is more sensitive to changes in CO_2 at higher elevations (Poulsen and Jeffery, 2011). Thus as Andean elevation has increased, $\delta^{18}O_{prec}$ has become more sensitive to smaller changes in CO_2.

Existing stable isotope records of $\delta^{18}O_{prec}$ are consistent with predictions of changes in $\delta^{18}O_{prec}$ due to Andean uplift and associated climate change. However, these records are also consistent with Andean uplift accompanied by changing CO_2 levels and inland seaway incursions, as well as local changes in temperature and evaporation rates. We therefore suggest alternative explanations for existing records, quantify uncertainties in paleoelevation estimates, and show that it is necessary to consider all of these factors when interpreting Cenozoic records of $\delta^{18}O_{prec}$ in South America.

ACKNOWLEDGMENTS

This work was funded by grants to C.J.P. and T.A.E. from National Science Foundation (EAR awards 0738822 and 0907817) and the University of Michigan's Graham Environmental Sustainability Institute. M.L.J. was also supported by a University of Michigan, Rackham International Student Fellowship. National Centers for Environmental Prediction (NCEP) reanalysis and the Climate Prediction Center (CPC) Merged Analysis of Precipitation (CMAP) data provided by the National Oceanic and Atmospheric Association (NOAA)–Office of Oceanic and Atmospheric Research (OAR)–Earth System Research Laboratory (ESRL)–Physical Sciences Division (PSD), Boulder, Colorado, USA, from their Web site at http://www.esrl.noaa.gov/psd/. This research benefited from discussions with Nadja Insel. We are grateful for comments by Page Chamberlain and an anonymous reviewer that helped to improve this manuscript.

REFERENCES CITED

Allmendinger, R.W., Jordan, T.E., Kay, S.M., and Isacks, B.L., 1997, The evolution of the Altiplano-Puna plateau of the central Andes: Annual Review of Earth and Planetary Sciences, v. 25, p. 139–174, doi:10.1146/annurev.earth.25.1.139.

Aravena, R., Suzuki, O., Pena, H., Pollastri, A., Fuenzalida, H., and Grilli, A., 1999, Isotopic composition and origin of the precipitation in northern Chile: Applied Geochemistry, v. 14, no. 4, p. 411–422, doi:10.1016/S0883-2927(98)00067-5.

Barnes, J.B., and Ehlers, T.A., 2009, End member models for Andean Plateau uplift: Earth-Science Reviews, v. 97, no. 1–4, p. 105–132, doi:10.1016/j.earscirev.2009.08.003.

Barnes, J.B., Ehlers, T.A., McQuarrie, N., O'Sullivan, P.B., and Tawackoli, S., 2008, Thermochronometer record of central Andean plateau growth, Bolivia (19.5 °S): Tectonics, v. 27, TC3003, 25 p., doi:10.1029/2007TC002174.

Bershaw, J., Garzione, C.N., Higgins, P., MacFadden, B.J., Anaya, F., and Alvarenga, H., 2010, Spatial-temporal changes in Andean plateau climate and elevation from stable isotopes of mammal teeth: Earth and Planetary Science Letters, v. 289, no. 3–4, p. 530–538, doi:10.1016/j.epsl.2009.11.047.

Blisniuk, P.M., Stern, L.A., Chamberlain, C.P., Idleman, B., and Zeitler, P.K., 2005, Climatic and ecologic changes during Miocene surface uplift in the southern Patagonian Andes: Earth and Planetary Science Letters, v. 230, no. 1–2, p. 125–142, doi:10.1016/j.epsl.2004.11.015.

Blisniuk, P.M., Stern, L.A., Chamberlain, C.P., Zeitler, P.K., Ramos, V.A., Sobel, E.R., Haschke, M., Strecker, M.R., and Warkus, F., 2006, Links between mountain uplift, climate, and surface processes in the southern Patagonian Andes, *in* Oncken, O., Chong, G., Franz, G., Giese, P., Götze, H.-J., Ramos, V. A., Strecker, M. R., and Wigger, P., eds., The Andes—Active Subduction Orogeny: Berlin, Heidelberg, Springer, p. 429–440.

Campetella, C.M., and Vera, C.S., 2002, The influence of the Andes mountains on the South American low-level flow: Geophysical Research Letters, v. 29, no. 17, 1826, 4 p., doi:10.1029/2002GL015451.

Cooper, M.A., Addison, F.T., Alvarez, R., Coral, M., Graham, R.H., Hayward, A.B., Howe, S., Martinez, J., Naar, J., Penas, R., Pulham, A.J., and Taborda, A., 1995, Basin development and tectonic history of the Llanos Basin, Eastern Cordillera, and middle Magdalena Valley, Colombia: American Association of Petroleum Geologists Bulletin, v. 79, p. 1421–1443.

Craig, H., and Gordon, L.I., 1965, Deuterium and oxygen 18 variations in the ocean and marine atmosphere, *in* Tongiorgi, E., ed., Stable Isotopes In Oceanography Studies and Paleotemperatures: Pisa, Laboratorio di Geologia Nucleare, p. 9–130.

Dansgaard, W., 1964, Stable isotopes in precipitation: Tellus, v. 16, no. 4, p. 436–468, doi:10.1111/j.2153-3490.1964.tb00181.x.

DeCelles, P.G., and Horton, B.K., 2003, Early to middle Tertiary foreland basin development and the history of Andean crustal shortening in Bolivia: Geological Society of America Bulletin, v. 115, no. 1, p. 58–77, doi:10.1130/0016-7606(2003)115<0058:ETMTFB>2.0.CO;2.

Demicco, R.V., Lowenstein, T.K., and Hardie, L.A., 2003, Atmospheric pCO(2) since 60 Ma from records of seawater pH, calcium, and primary carbonate mineralogy: Geology, v. 31, no. 9, p. 793–796, doi:10.1130/G19727.1.

Dorman, J.L., and Sellers, P.J., 1989, A global climatology of albedo, roughness length and stomatal-resistance for atmospheric general-circulation models as represented by the simple biosphere model (SIB): Journal of Applied Meteorology, v. 28, no. 9, p. 833–855, doi:10.1175/1520-0450(1989)028<0833:AGCOAR>2.0.CO;2.

Ehlers, T.A., and Poulsen, C.J., 2009, Influence of Andean uplift on climate and paleoaltimetry estimates: Earth and Planetary Science Letters, v. 281, no. 3–4, p. 238–248, doi:10.1016/j.epsl.2009.02.026.

Ehrmann, W.U., and Mackensen, A., 1992, Sedimentological evidence for the formation of an east Antarctic ice-sheet in Eocene–Oligocene time: Palaeogeography, Palaeoclimatology, Palaeoecology, v. 93, no. 1–2, p. 85–112, doi:10.1016/0031-0182(92)90185-8.

Epstein, S., and Mayeda, T., 1953, Variation of ^{18}O content of waters from natural sources: Geochimica et Cosmochimica Acta, v. 4, no. 5, p. 213–224, doi:10.1016/0016-7037(53)90051-9.

Ferronsky, V.I., and Brezgunov, V.S., 1989, Stable isotopes and ocean dynamics, *in* Fritz, P., and Fontes, J., eds., Handbook of Environmental Isotope Geochemistry, Volume 3: New York, Elsevier Science, p. 1–73.

Frailey, C.D., Lavina, E.L., Rancy, A., and de Souza Filho, J.P., 1988, A proposed Pleistocene–Holocene lake in the Amazon basin and its significance to Amazonian geology and biogeography: Acta Amazonica, v. 18, p. 119–143.

Garzione, C., Hoke, G.D., Libarkin, J.C., Withers, S., MacFadden, B.J., Eiler, J., Ghosh, P., and Mulch, A., 2008, Rise of the Andes: Science, v. 320, no. 5881, p. 1304–1307, doi:10.1126/science.1148615.

Garzione, C.N., Molnar, P., Libarkin, J.C., and MacFadden, B.J., 2006, Rapid late Miocene rise of the Bolivian Altiplano: Evidence for removal of mantle lithosphere: Earth and Planetary Science Letters, v. 241, no. 3–4, p. 543–556, doi:10.1016/j.epsl.2005.11.026.

Gat, J.R., 1996, Oxygen and hydrogen isotopes in the hydrologic cycle: Annual Review of Earth and Planetary Sciences, v. 24, p. 225–262, doi:10.1146/annurev.earth.24.1.225.

Ghosh, P., Garzione, C.N., and Eiler, J.M., 2006, Rapid uplift of the Altiplano revealed through ^{13}C-^{18}O bonds in paleosol carbonates: Science, v. 311, no. 5760, p. 511–515, doi:10.1126/science.1119365.

Gingras, M.K., Rasanen, M.E., Pemberton, S.G., and Romero, L.P., 2002, Ichnology and sedimentology reveal depositional characteristics of bay-margin parasequences in the Miocene Amazonian foreland basin: Journal of Sedimentary Research, v. 72, no. 6, p. 871–883, doi:10.1306/052002720871.

Giovanni, M.K., Horton, B.K., Garzione, C., McNulty, B., and Grove, M., 2010, Extensional basin evolution in

the Cordillera Blanca, Peru: Stratigraphic and isotopic records of detachment faulting and orogenic collapse in the Andean hinterland: Tectonics, v. 29, TC6007, 21 p., doi:10.1029/2010TC002666.

Gómez, E., Jordan, T.E., Allmendinger, R.W., and Cardozo, N., 2005, Development of the Colombian foreland-basin system as a consequence of diachronous exhumation of the northern Andes: Geological Society of America Bulletin, v. 117, no. 9–10, p. 1272–1292, doi:10.1130/B25456.1.

Gonfiantini, R., Roche, M.A., Olivry, J.C., Fontes, J.C., and Zuppi, G.M., 2001, The altitude effect on the isotopic composition of tropical rains: Chemical Geology, v. 181, no. 1–4, p. 147–167, doi:10.1016/S0009-2541(01)00279-0.

Hartley, A.J., 2003, Andean uplift and climate change: Journal of the Geological Society, v. 160, p. 7–10, doi:10.1144/0016-764902-083.

Hernandez, R.M., Jordan, T.E., Farjat, A.D., Echavarria, L., Idleman, B.D., and Reynolds, J.H., 2005, Age, distribution, tectonics, and eustatic controls of the Paranense and Caribbean marine transgressions in southern Bolivia and Argentina: Journal of South American Earth Sciences, v. 19, no. 4, p. 495–512, doi:10.1016/j.jsames.2005.06.007.

Hoke, G.D., Garzione, C.N., Araneo, D.C., Latorre, C., Strecker, M.R., and Williams, K.J., 2009, The stable isotope altimeter: Do Quaternary pedogenic carbonates predict modern elevations?: Geology, v. 37, no. 11, p. 1015–1018, doi:10.1130/G30308A.1.

Hoorn, C., 2006, Mangrove forests and marine incursions in Neogene Amazonia (lower Apaporis River, Colombia): Palaios, v. 21, no. 2, p. 197–209, doi:10.2110/palo.2005.p05-131.

Hoorn, C., Wesselingh, F.P., Hovikoski, J., and Guerrero, J., 2010, The development of the Amazonian mega-wetland (Miocene; Brazil, Colombia, Peru, Bolivia), *in* Hoorn, C., and Wesselingh, F.P., eds., Amazonia, Landscape and Species Evolution: A Look into the Past: Oxford, UK, Wiley-Blackwell Publishing, p. 123–142.

Houston, J., and Hartley, A.J., 2003, The central Andean west-slope rain shadow and its potential contribution to the origin of hyper-aridity in the Atacama Desert: International Journal of Climatology, v. 23, no. 12, p. 1453–1464, doi:10.1002/joc.938.

Hovikoski, J., Rasanen, M., Gingras, M., Roddaz, M., Brusset, S., Hermoza, W., and Pittman, L.R., 2005, Miocene semidiurnal tidal rhythmites in Madre de Dios, Peru: Geology, v. 33, no. 3, p. 177–180, doi:10.1130/G21102.1.

Hovikoski, J., Gingras, M., Rasanen, M., Rebata, L.A., Guerrero, J., Ranzi, A., Melo, J., Romero, L., del Prado, H.N., Jaimes, F., and Lopez, S., 2007, The nature of Miocene Amazonian epicontinental embayment: High-frequency shifts of the low-gradient coastline: Geological Society of America Bulletin, v. 119, no. 11–12, p. 1506–1520.

Hovikoski, J., Wesselingh, F.P., Rasanen, M., Gingras, M., and Vonhof, H.B., 2010, Marine influence in Amazonia: Evidence from the geological record, *in* Hoorn, C., and Wesselingh, F.P., eds., Amazonia, Landscape and Species Evolution: A Look into the Past: Oxford, UK, Wiley-Blackwell Publishing, p. 143–161.

Insel, N., Poulsen, C. J., and Ehlers, T. A., 2009, Influence of the Andes Mountains on South American moisture transport, convection, and precipitation: Climate Dynamics, v. 35, p. 1477–1492.

International Atomic Energy Agency–World Meteorological Organization, 2006, Global network of isotopes in precipitation (GNIP) database: http://www.iaea.org/water (August 2009).

Isacks, B.L., 1988, Uplift of the central Andean plateau and bending of the Bolivian orocline: Journal of Geophysical Research, Solid Earth and Planets, v. 93, no. B4, p. 3211–3231, doi:10.1029/JB093iB04p03211.

Kalnay, E., Kanamitsu, M., Kistler, R., Collins, W., Deaven, D., Gandin, L., Iredell, M., Saha, S., White, G., Woollen, J., Zhu, Y., Chelliah, M., Ebisuzaki, W., Higgins, W., Janowiak, J., Mo, K.C., Ropelewski, C., Wang, J., Leetmaa, A., Reynolds, R., Jenne, R., and Joseph, D., 1996, The NCEP/NCAR 40-year reanalysis project: Bulletin of the American Meteorological Society, v. 77, no. 3, p. 437–471, doi:10.1175/1520-0477(1996)077<0437:TNYRP>2.0.CO;2.

Kim, S.T., and Oneil, J.R., 1997, Equilibrium and nonequilibrium oxygen isotope effects in synthetic carbonates: Geochimica et Cosmochimica Acta, v. 61, no. 16, p. 3461–3475, doi:10.1016/S0016-7037(97)00169-5.

Kleinert, K., and Strecker, M.R., 2001, Climate change in response to orographic barrier uplift: Paleosol and stable isotope evidence from the late Neogene Santa Maria basin, northwestern Argentina: Geological Society of America Bulletin, v. 113, no. 6, p. 728–742, doi:10.1130/0016-7606(2001)113<0728:CCIRTO>2.0.CO;2.

Knutti, R., Meehl, G.A., Allen, M.R., and Stainforth, D.A., 2006, Constraining climate sensitivity from the seasonal cycle in surface temperature: Journal of Climate, v. 19, no. 17, p. 4224–4233, doi:10.1175/JCLI3865.1.

Kurschner, W.M., Kvacek, Z., and Dilcher, D.L., 2008, The impact of Miocene atmospheric carbon dioxide fluctuations on climate and the evolution of terrestrial ecosystems: Proceedings of the National Academy of Sciences of the United States of America, v. 105, no. 2, p. 449–453, doi:10.1073/pnas.0708588105.

Latorre, C., Quade, J., and McIntosh, W.C., 1997, The expansion of C-4 grasses and global change in the late Miocene: Stable isotope evidence from the Americas: Earth and Planetary Science Letters, v. 146, no. 1–2, p. 83–96, doi:10.1016/S0012-821X(96)00231-2.

Latrubesse, E.M., Cozzuol, M., da Silva-Caminha, S.A.F., Rigsby, C.A., Absy, M.L., and Jaramillo, C., 2010, The Late Miocene paleogeography of the Amazon Basin and the evolution of the Amazon River system: Earth-Science Reviews, v. 99, no. 3–4, p. 99–124, doi:10.1016/j.earscirev.2010.02.005.

Lear, C.H., Elderfield, H., and Wilson, P.A., 2000, Cenozoic deep-sea temperatures and global ice volumes from Mg/Ca in benthic foraminiferal calcite: Science, v. 287, no. 5451, p. 269–272, doi:10.1126/science.287.5451.269.

Lenters, J.D., and Cook, K.H., 1995, Simulation and diagnosis of the regional summertime precipitation climatology of South America: Journal of Climate, v. 8, no. 12, p. 2988–3005, doi:10.1175/1520-0442(1995)008<2988:SADOTR>2.0.CO;2.

Lovejoy, N.R., Albert, J.S., and Crampton, W.G.R., 2006, Miocene marine incursions and marine/freshwater transitions: Evidence from Neotropical fishes: Journal of South American Earth Sciences, v. 21, no. 1–2, p. 5–13, doi:10.1016/j.jsames.2005.07.009.

Mathieu, R., Pollard, D., Cole, J.E., White, J.W.C., Webb, R.S., and Thompson, S.L., 2002, Simulation of stable water isotope variations by the GENESIS GCM for modern conditions: Journal of Geophysical Research–Atmospheres, v. 107, no. D4, p. 2-1–2-18.

Matthews, R.K., and Poore, R.Z., 1980, Tertiary $\delta^{18}O$ record and glacio-eustatic sea-level fluctuations: Geology, v. 8, no. 10, p. 501–504, doi:10.1130/0091-7613(1980)8<501:TORAGS>2.0.CO;2.

McQuarrie, N., 2002, The kinematic history of the central Andean fold-thrust belt, Bolivia: Implications for building a high plateau: Geological Society of America Bulletin, v. 114, no. 8, p. 950–963, doi:10.1130/0016-7606(2002)114<0950:TKHOTC>2.0.CO;2.

McQuarrie, N., Horton, B.K., Zandt, G., Beck, S., and DeCelles, P.G., 2005, Lithospheric evolution of the Andean fold-thrust belt, Bolivia, and the origin of the central Andean plateau: Tectonophysics, v. 399, no. 1–4, p. 15–37, doi:10.1016/j.tecto.2004.12.013.

Miller, K.G., Fairbanks, R.G., and Mountain, G.S., 1987, Tertiary oxygen isotope synthesis, sea-level history, and continental margin erosion: Paleoceanography, v. 2, p. 1–19, doi:10.1029/PA002i001p00001.

Mulch, A., Uba, C.E., Strecker, M.R., Schoenberg, R., and Chamberlain, C.P., 2010, Late Miocene climate variability and surface elevation in the central Andes: Earth and Planetary Science Letters, v. 290, no. 1–2, p. 173–182, doi:10.1016/j.epsl.2009.12.019.

Murphy, J.M., Sexton, D.M.H., Barnett, D.N., Jones, G.S., Webb, M.J., and Collins, M., 2004, Quantification of modelling uncertainties in a large ensemble of climate change simulations: Nature, v. 430, no. 7001, p. 768–772, doi:10.1038/nature02771.

Ostlund, H.G., Craig, H., Broecker, W.S., and Spencer, D., 1987, Shore-based data and graphics: Atlantic, Pacific, and Indian Ocean Expeditions: Washington, D.C., National Science Foundation Geochemical Ocean Sections Study, v. 7.

Pagani, M., Zachos, J.C., Freeman, K.H., Tipple, B., and Bohaty, S., 2005, Marked decline in atmospheric carbon dioxide concentrations during the Paleogene: Science, v. 309, no. 5734, p. 600–603, doi:10.1126/science.1110063.

Parra, M., Mora, A., Jaramillo, C., Torres, V., Zeilinger, G., and Strecker, M.R., 2010, Tectonic controls on Cenozoic foreland basin development in the northeastern Andes, Colombia: Basin Research, v. 22, no. 6, p. 874–903.

Pearson, P.N., and Palmer, M.R., 2000, Atmospheric carbon dioxide concentrations over the past 60 million years: Nature, v. 406, no. 6797, p. 695–699, doi:10.1038/35021000.

Pearson, P.N., Foster, G.L., and Wade, B.S., 2009, Atmospheric carbon dioxide through the Eocene–Oligocene climate transition: Nature, v. 461, no. 7267, p. 1110–1113, doi:10.1038/nature08447.

Poage, M.A., and Chamberlain, C.P., 2001, Empirical relationships between elevation and the stable isotope composition of precipitation and surface waters: Considerations for studies of paleoelevation change: American Journal of Science, v. 301, no. 1, p. 1–15, doi:10.2475/ajs.301.1.1.

Poulsen, C.J., Ehlers, T.A., and Insel, N., 2010, Onset of convective rainfall during gradual late Miocene rise of the central Andes: Science, v. 328, no. 5977, p. 490–493, doi:10.1126/science.1185078.

Poulsen, C.J., and Jeffery, M.L., 2011, Climate change imprinting on stable isotopic compositions of high-elevation meteoric water cloaks past surface elevations of major orogens, *Geology*, 39, p. 595–598, doi:10.1130/632052.1

Quade, J., Cerling, T.E., and Bowman, J.R., 1989, Systematic variations in the carbon and oxygen isotopic composition of pedogenic carbonate along elevation transects in the southern Great Basin, United States: Geological Society of America Bulletin, v. 101, no. 4, p. 464–475, doi:10.1130/0016-7606(1989)101<0464:SVITCA>2.3.CO;2.

Ramos, V.A., Cristallini, E.O., and Perez, D.J., 2002, The Pampean flat-slab of the central Andes: Journal of South American Earth Sciences, v. 15, no. 1, p. 59–78, doi:10.1016/S0895-9811(02)00006-8.

Rasanen, M.E., Linna, A.M., Santos, J.C.R., and Negri, F.R., 1995, Late Miocene tidal deposits in the Amazonian foreland basin: Science, v. 269, no. 5222, p. 386–390, doi:10.1126/science.269.5222.386.

Rech, J.A., Currie, B.S., Shullenberger, E.D., Dunagan, S.P., Jordan, T.E., Blanco, N., Tomlinson, A.J., Rowe, H.D., and Houston, J., 2010, Evidence for the development of the Andean rain shadow from a Neogene isotopic record in the Atacama Desert, Chile: Earth and Planetary Science Letters, v. 292, no. 3–4, p. 371–382, doi:10.1016/j.epsl.2010.02.004.

Ropelewski, C.F., and Halpert, M.S., 1987, Global and regional scale precipitation patterns associated with the El Nino–Southern Oscillation: Monthly Weather Review, v. 115, no. 8, p. 1606–1626, doi:10.1175/1520-0493(1987)115<1606:GARSPP>2.0.CO;2.

Royer, D.L., 2006, CO_2-forced climate thresholds during the Phanerozoic: Geochimica et Cosmochimica Acta, v. 70, no. 23, p. 5665–5675, doi:10.1016/j.gca.2005.11.031.

Rozanski, K., Araguas-Araguas, L., and Gonfiantini, R., 1993, Isotopic patterns in modern global precipitation, *in* Swart, P.K., Lohmann, K.C., McKenzie, J.A.,, and Savin, S., eds., American Geophysical Union Monograph, v. 78, p. 1–36.

Salati, E., Attilio, D.O., Matsui, E., and Gat, J.R., 1979, Recycling of water in the Amazon Basin: An isotopic study: Water Resources Research, v. 15, no. 5, p. 1250–1258, doi:10.1029/WR015i005p01250.

Sheldon, N.D., 2006, Using paleosols of the Picture Gorge Basalt to reconstruct the middle Miocene climatic optimum: Paleobios, v. 26, no. 2, p. 27–36.

Siegert, M.J., Barrett, P., Decont, R., Dunbar, R., Cofaigh, C.O., Passchier, S., and Naish, T., 2008, Recent advances in understanding Antarctic climate evolution:

Antarctic Science, v. 20, no. 4, p. 313–325, doi:10.1017/S0954102008000941.

Sloan, L.C., Crowley, T.J., and Pollard, D., 1996, Modeling of middle Pliocene climate with the NCAR GENESIS general circulation model: Marine Micropaleontology, v. 27, no. 1–4, p. 51–61, doi:10.1016/0377-8398(95)00063-1.

Smith, A.G., Hurley, A.M., and Briden, J.C., 1981, Phanerozoic paleocontinental world maps: Cambridge, UK, Cambridge University Press, Cambridge Earth Science Series, 107 p.

Stern, L.A., and Blisniuk, P.M., 2002, Stable isotope composition of precipitation across the southern Patagonian Andes: Journal of Geophysical Research-Atmospheres, v. 107, no. D23.

Sturm, C., Hoffmann, G., and Langmann, B., 2007, Simulation of the stable water isotopes in precipitation over South America: Comparing regional to global circulation models: Journal of Climate, v. 20, no. 15, p. 3730–3750, doi:10.1175/JCLI4194.1.

Taboada, A., Rivera, L.A., Fuenzalida, A., Cisternas, A., Philip, H., Bijwaard, H., Olaya, J., and Rivera, C., 2000, Geodynamics of the northern Andes: Subductions and intracontinental deformation (Colombia): Tectonics, v. 19, no. 5, p. 787–813, doi:10.1029/2000TC900004.

Thompson, S.L., and Pollard, D., 1995, A global climate model (GENESIS) with a land-surface transfer scheme (LSX). 1. Present climate simulation: Journal of Climate, v. 8, no. 4, p. 732–761, doi:10.1175/1520-0442(1995)008<0732:AGCMWA>2.0.CO;2.

Thompson, S.L., and Pollard, D., 1997, Greenland and Antarctic mass balances for present and doubled atmospheric CO_2 from the GENESIS version-2 global climate model: Journal of Climate, v. 10, no. 5, p. 871–900, doi:10.1175/1520-0442(1997)010<0871:GAAMBF>2.0.CO;2.

Thomson, S., Hervé, F., and Stöckhert, B., 2001, Mesozoic–Cenozoic denudation history of the Patagonian Andes (southern Chile) and its correlation to different subduction processes: Tectonics, v. 20, no. 5, p. 693–711, doi:10.1029/2001TC900013.

Uba, C.E., Hasler, C.A., Buatois, L.A., Schmitt, A.K., and Plessen, B., 2009, Isotopic, paleontologic, and ichnologic evidence for late Miocene pulses of marine incursions in the central Andes: Geology, v. 37, no. 9, p. 827–830, doi:10.1130/G30014A.1.

Vuille, M., Bradley, R.S., Werner, M., Healy, R., and Keimig, F., 2003, Modeling $\delta^{18}O$ in precipitation over the tropical Americas: 1. Interannual variability and climatic controls: Journal of Geophysical Research—Atmospheres, v. 108, no. D6.

Wesselingh, F.P., Rasanen, M.E., Irion, G., Vonhof, H.B., Kaandorp, R.J.G., Renema, W., Romero Pittman, L., and Gingras, M., 2002, Lake Pebas: A palaeoecological reconstruction of a Miocene, long-lived lake complex in western Amazonia: Cainozoic Research, v. 1, p. 35–81.

Wesselingh, F.P., Kaandorp, R.J.G., Vonhof, H.B., Rasanen, M., and Renema, W., 2006, The nature of aquatic landscapes in the Miocene of western Amazonia: An integrated palaeontological and geochemical approach: Scripta Geologica, no. 133, p. 363–393.

Xie, P.P., and Arkin, P.A., 1997, Global precipitation: A 17-year monthly analysis based on gauge observations, satellite estimates, and numerical model outputs: Bulletin of the American Meteorological Society, v. 78, no. 11, p. 2539–2558, doi:10.1175/1520-0477(1997)078<2539:GPAYMA>2.0.CO;2.

Zachos, J.C., Breza, J.R., and Wise, S.W., 1992, Early Oligocene ice-sheet expansion on Antarctica—Stable isotope and sedimentological evidence from Kerguelen Plateau, southern Indian Ocean: Geology, v. 20, no. 6, p. 569–573, doi:10.1130/0091-7613(1992)020<0569:EOISEO>2.3.CO;2.

Zhou, J., Poulsen, C.J., Pollard, D., and White, T.S., 2008, Simulation of modern and middle Cretaceous marine $\delta^{18}O$ with an ocean-atmosphere general circulation model: Paleoceanography, v. 23, PA3223, 11 p., doi:10.1029/2008PA001596.

Science Editor: A. Hope Jahren
Associate Editor: David R. Marchant

Manuscript Received 6 January 2011
Revised Manuscript Received 6 June 2011
Manuscript Accepted 14 June 2011

Printed in the USA